

1
2
3
4
5
6
7
8
9
10
11
12
13
14
15
16
17

**Medium-range predictability of early summer sea ice thickness distribution in the East Siberian Sea based on the TOPAZ4 ice-ocean data assimilation system:
~~Importance of dynamical and thermodynamic melting processes~~**

Takuya Nakanowatari^{1,*}, Jun Inoue¹, Kazutoshi Sato¹, Laurent Bertino², Jiping Xie², Mio Matsueda³, Akio Yamagami³, Takeshi Sugimura¹, Hironori Yabuki¹, and Natsuhiko Otsuka⁴

¹National Institute of Polar Research, 10-3, Midori-cho, Tachikawa-shi, Tokyo, 190-8518, Japan;

²Nansen Environmental and Remote Sensing Center, Thormøhlens gate 47, N-5006 Bergen,

Norway; ³Center for Computational Sciences, University of Tsukuba, 1-1-1 Tennodai, Tsukuba,

Ibaraki 305-8577, Japan; ⁴Arctic Research Center, Hokkaido University, Kita-21 Nishi-11 Kita-ku,

Sapporo, 001-0021, Japan

*Corresponding author: Takuya Nakanowatari, E-mail: nakanowatari.takuya@nipr.ac.jp

Abstract

Accelerated retreat of Arctic Ocean summertime sea ice has focused attention on the potential use of the Northern Sea Route (NSR), for which sea ice thickness (SIT) information is crucial for safe maritime navigation. This study evaluated the medium-range (lead time below 10 days) forecast skill of SIT distribution in the East Siberian Sea (ESS) in early summer (June–July) based on the TOPAZ4 ice ocean data assimilation system. Comparison of the operational model SIT data to reliable SIT estimates (hindcast, satellite, and in situ data)~~all available observations (in situ and satellite)~~ showed that the TOPAZ4 reanalysis reproduces qualitatively the tongue-like distribution of SIT in ESS in early summer and the seasonal variations~~observed seasonal cycle and the rates of advance and melting of SIT in the ESS, with average bias of approximately ± 20 cm~~. Pattern correlation analysis of the SIT forecast data over 34 years (~~2014~~~~2013~~–2016) reveals that the early summer SIT distribution is skillfully predicted for a lead time of up to 3 days, but that the prediction skill drops abruptly after the 4th day, which is related to dynamical process controlled by synoptic-scale atmospheric fluctuations. For longer lead times (>4 days), the thermodynamic melting process takes over, which makes most of the remaining prediction skill. In July 2014, during which an ice-blocking incident occurred, relatively thick SIT (~ 150 cm) was simulated over the ESS, which is consistent with the reduction of vessel speed. These results suggest that TOPAZ4 sea ice information has a great potential for practical applications in summertime maritime navigation via the NSR.

38 **1 Introduction**

39 During recent decades, sea ice cover in the Northern Hemisphere has shown remarkable
40 reduction and the largest rates of decrease of $100,000 \text{ km}^2 \text{ decade}^{-1}$ has been observed in the
41 western Arctic Ocean in summer [Cavalieri and Parkinson, 2008]. Sea ice retreat influences the
42 light conditions for phytoplankton photosynthesis activity [Wassmann, 2011], and the resultant
43 meltwater influences the marine environment via ocean acidification [Yamamoto-Kawai et al.,
44 2011]. In winter, shrinkage of the sea ice area in marginal seas, such as the Barents Sea changes the
45 surface boundary conditions of the atmosphere, influences planetary waves, and causes blocking
46 events that are one of the possible causes of the recent severe winters in mid-latitude regions
47 [Honda et al., 2009; Inoue et al., 2012; Mori et al., 2014; Overland et al., 2015; Petoukhov and
48 Semenov, 2010; Screen, 2017].

49 In contrast to these climatic consequences and problems for the marine ecosystem caused by
50 the reduction in sea ice, the retreat of Arctic sea ice has new opportunities for commercial maritime
51 navigation. It has been reported that exploitation of shipping routes in the Arctic Ocean, i.e., the
52 Northern Sea Route (NSR), could reduce the navigational distance between Europe and Asia by
53 about 40% in comparison with routes via the Suez Canal [Schøyen and Bråthen, 2011]. Melia et al.
54 [2016] discussed the possibility of a viable trans-Arctic shipping route in the 21st century, based on
55 the Coupled Model Intercomparison Project Phase 5 ([CMIP5](#)) global climate model simulation.
56 Currently, the summertime use of the NSR by commercial vessels such as cargo ships and tankers
57 has increased [Eguíluz et al., 2016]. Therefore, obtaining precise information on sea ice condition
58 and evaluating the forecast skill of operational sea ice models have become urgent issues.

59 Many previous studies have examined the predictability of summertime sea ice change in the
60 Arctic Ocean in terms of its coverage [Wang et al., 2013] and motion [Schweiger and Zhang, 2015].
61 Kimura et al. [2013] reported a good correlation of the spatial distribution of summertime sea ice
62 concentration (SIC) with winter ice divergence/convergence. Their study indicated that sea ice

63 thickness (SIT) or sea ice volume before the melt season is a source of predictability for
64 summertime SIC. Recently, their study was supported by hindcast experiments undertaken using a
65 climate model, in which the SIC in the East Siberian Sea (ESS) was shown to have significant
66 seasonal prediction skill [Bushuk et al., 2017]. The significant impacts of SIT condition on the
67 seasonal prediction of SIC in the Arctic Ocean have been highlighted by many studies [Lindsay et
68 al., 2008; Holland et al., 2011; Blanchard-Wrigglesworth and Bitz, 2014; Collow et al., 2015; Melia
69 et al., 2015; Chen et al. 2017; Melia et al. 2017]. Thus, the persistence of SIT or sea ice volume is
70 one of the key factors determining the skill of seasonal predictions of summertime sea ice area.

71 Earlier studies have focused primarily on the seasonal to interannual predictability of SIC or
72 sea ice area in the Arctic Ocean; thus, subseasonal variation in SIT and its predictability have not
73 been examined fully for near-term route planning. Although the summertime sea ice extent has
74 rapidly decreased on interannual timescale, substantial sea ice area still remains in critical stretches
75 of the NSR such as the ESS in early summer (June–July). Since precise information regarding SIT
76 and its near-future condition is crucial for icebreaker operations [Tan et al., 2013; Pastusiak, 2016],
77 it is important to clarify the medium-range (3 to 10 days lead time) predictability of summertime
78 SIT in the Arctic Ocean.

79 Synoptic-scale fluctuations of cyclone and anticyclone is greater over the Arctic Ocean and
80 Eurasia in summer than in winter [Serreze and Barry, 1988; Serreze and Barrett, 2008]. In recent
81 years, there is a risk that an Arctic cyclone becomes extremely developed and covered the entire
82 Pacific sector [Simmonds and Rudeva, 2012; Yamagami et al. 2017]. Because the ESS corresponds
83 to the route of Arctic cyclones generated over the Eurasian Continent [Orsolini and Sorteberg,
84 2009], it is expected that synoptic-scale atmospheric fluctuations would influence substantially the
85 spatial distribution of SIT and ice motion in the ESS. Ono et al. [2016] highlighted the importance
86 of atmospheric prediction skill on medium-range forecasts of sea ice distribution in the ESS based
87 on a case of an extreme cyclone that occurred on 6 August 2012. On the other hand, earlier studies

88 pointed out that the sea ice melting process is important for the long-term prediction of summertime
89 sea ice extent [e.g., Bushuk et al., 2017]. But the relative importance of dynamical and
90 thermodynamic processes on the medium-range forecast skill of summertime sea ice properties has
91 not yet been well understood.

92 Since 2010, ice–ocean forecasts and a 20-years reanalysis are available for the Arctic Ocean,
93 based on the TOPAZ ocean data assimilation system (Towards an Operational Prediction system for
94 the North Atlantic European coastal Zones) in its 4th version [Sakov et al., 2012]. The Norwegian
95 Meteorological Institute provides 10-day forecast products in daily mean fields, forced at the
96 surface by the [European Centre for Medium-Range Weather Forecasts \(ECMWF\)](#) ~~ECMWF~~
97 operational atmospheric forecasts, updated daily and distributed by the Copernicus Marine
98 Environment Monitoring Services (<http://marine.copernicus.eu>). The reliability of the
99 corresponding TOPAZ4 reanalysis data has been evaluated previously through comparison with in
100 situ and satellite SIT data [Xie et al. 2017; ~~Nakanowatari et al. 2017~~]. They showed the SIT in the
101 TOPAZ4 reanalysis data are comparable to observed values over the Beaufort Gyre and central
102 Arctic Ocean, although the SIT overall shows a negative bias of several dozen centimeters
103 throughout a year. Thus, it is expected that the SIT data in the TOPAZ reanalysis data should also
104 be reliable in the ESS even in the melting season, and the forecast SIT data should show skillful
105 prediction skill on medium-range time scale.

106 In this study, we examined the predictability of the early summer SIT distribution in the ESS
107 on the medium-range timescale and discussed its underlying physical mechanisms, based on the
108 TOPAZ4 forecast dataset and trivial dynamical and thermodynamical models. Section 2 describes
109 the data and methods. Section 3 evaluates the reliability of the SIT data in the TOPAZ4 reanalysis
110 data through comparison with all available in situ and satellite observations, as well as operational
111 model analyses, with particular emphasis on the ESS. In section 4, we examine the predictability of
112 the SIT distribution in the ESS based on TOPAZ4 forecast data. Section 5 examines the relationship

113 between sea ice conditions and vessel speed during an ice-blocking event that occurred in July 2014.

114 A discussion and the derived conclusions are presented in section 6.

115

116 **2 Data and Methods**

117 This study used daily mean sea ice data derived from the TOPAZ4 Arctic sea ice forecast
118 system dataset, in which the SSM/I SIC data, hydrographic temperature and salinity data,
119 along-track sea level anomaly, and satellite estimates of ice drift and sea surface temperature were
120 assimilated, but sea ice thickness was not yet assimilated in this version of the reanalysis [Simonsen
121 et al. 2017]. The TOPAZ4 system was designed as a regional ice–ocean coupled system forced with
122 atmospheric flux data. The ocean model of TOPAZ4 is based on version 2.2 of HYCOM, which
123 uses isopycnical vertical coordinates in the ocean interior and z level coordinates in the near-surface
124 layer. The sea ice model uses an elastic–viscous–plastic rheology [Hunke and Dukowicz, 1997].
125 The thermodynamic processes are based on a three-layer thermodynamic model with one snow and
126 2 ice layers [Semtner, 1976] with a modification for subgrid-scale ice thickness heterogeneities
127 [Fichefet and Morales Maqueda, 1997]. The model domain covers the Arctic Ocean and the North
128 Atlantic, and the lateral boundaries are relaxed to monthly mean climatological data. The spatial
129 resolution is 12–16 km with 28 hybrid layers, which constitutes eddy-permitting resolution in low-
130 and mid-latitude regions but not in the Arctic Ocean. [In this system, in situ hydrographic
131 observations are assimilated together with satellite observations of the ocean such as sea surface
132 temperature and sea level anomaly. Since this system assimilates the SIC and sea ice velocity \(but
133 the latter only in cold season\), one should expect adequate simulation of SIT through the ridging
134 process \[Stark et al. 2008\].](#) It has been reported that the SIT of the TOPAZ4 reanalysis data has
135 substantial negative bias from 2001 to 2010 due to excessive snowfall, which has been modified
136 after 2011 [Xie et al., 2017]. Therefore, this study used SIT data from 1 January 2011 to 31
137 December 2014.

138 The data assimilation method of TOPAZ4 is a deterministic version of the ensemble Kalman
139 filter (EnKF) [Sakov and Oke, 2008] with an ensemble of 100 dynamical members. Since EnKFs
140 have time-dependent state error covariances, this method is suitable for data assimilation of
141 anisotropic variables in areas close to the sea ice edge [Lisæter et al. 2003, Sakov et al. 2012]. ~~In~~
142 ~~this system, in situ hydrographic observations are assimilated together with satellite observations of~~
143 ~~the ocean such as sea surface temperature and sea surface height. Since this system assimilates the~~
144 ~~SIC and sea ice velocity (but the latter only in cold season), one should expect adequate simulation~~
145 ~~of SIT through the ridging process [Stark et al. 2008].~~ The TOPAZ4 reanalysis data were produced
146 with the 6-hourly forcing from ~~forced with 6 hourly atmospheric fluxes from~~ the ERA Interim
147 reanalysis [Dee et al., 2011]. The surface turbulent heat flux and momentum flux were both
148 calculated using bulk formula parameterizations [Kara et al., 2000; Large and Pond, 1981]; thus,
149 instead of the ERA-Interim fluxes themselves ~~fluxes derived from the atmospheric model were not~~
150 ~~used~~. The forecast and reanalysis systems have almost the same settings and their results are similar
151 during their overlap period (not shown).

152 To evaluate the prediction skill of the TOPAZ4 forecast system, we used daily mean sea ice
153 forecast data during 3 recent years from ~~2014~~2012 to 2016 [Simonsen et al. 2017]. A probabilistic
154 10-member ensemble forecast was performed with the ECMWF medium-range (up to 10 days)
155 atmospheric forecast data updated daily, out of which only the ensemble average is used. To
156 produce 10 ensemble members in the TOPAZ4 forecast system, the ECMWF global atmospheric
157 forecast data as well as several parameters of sea ice model are perturbed by adding stochastic
158 forcing term [Evensen, 2003]. ~~We excluded the forecast data of 2012 in this study, because the sea~~
159 ~~ice coverage of the ESS in early summer was quite small.~~ In this study, we excluded the forecast
160 data in July 2014, because of a real-time forecast production incident (the forecast were in
161 free-running mode then) [H. Engedahl, personal communication]-. Since the forecast data were only
162 provided weekly before 2016, the total of 150 cases was assembled during the study period. ~~Since~~

163 ~~the forecast data were only provided weekly before 2016, the total of 259 cases was assembled~~
164 ~~during the study period.~~ The skill core was quantified using pattern correlation coefficients (PCCs),
165 which are used widely in deterministic forecast verification [Barnett and Schlesinger, 1987]:

$$166 \quad PCC = \frac{\sum_{ij=1}^N (f_{ij} - \bar{f}_{ij})(a_{ij} - \bar{a}_{ij})}{\sqrt{\sum_{ij=1}^N (f_{ij} - \bar{f}_{ij})^2} \sqrt{\sum_{ij=1}^N (a_{ij} - \bar{a}_{ij})^2}} \quad (1)$$

167 where f_{ij} and a_{ij} are forecast and analysis sea ice variables, respectively. The overbar denotes the
168 average values over the analyzed area (see Fig. 1a); thus the PCC reflects the correlation of
169 observed and signal anomalies relative to their respective spatial means.

170 To evaluate the reliability of the SIT values in the TOPAZ4 reanalysis data in early summer,
171 we mainly ~~As an alternative model reanalysis, we~~ used the Pan-Arctic Ice Ocean Modeling and
172 Assimilation System (PIOMAS) outputs, which are derived from the coupled ice-ocean modeling
173 and assimilation system based on the Parallel Ocean Program POP and the Thickness and Enthalpy
174 Distribution (TED) sea ice model, forced with NCEP-NCAR reanalysis data [Zhang et al., 2003]. In
175 this dataset, SIC and sea surface temperature are assimilated by adoptive nudging, and many studies
176 [Schweiger et al., 2011; Lindsay and Zhang, 2006; Stroeve et al., 2014] have compared PIOMAS
177 output with observed SIT data and found it the most reliable estimate of observed SIT in the Arctic
178 Ocean [Laxon et al., 2013; Wang et al. 2016]. ~~The temporal and horizontal resolutions of the~~
179 ~~observed and simulated SIT data are summarized in Table 1. Before comparing the gridded SIT~~
180 ~~data with IMB buoy data in each grid point, we reconstructed these SIT data on a 0.25° latitude-~~
181 ~~longitude grid by applying bilinear interpolation.~~

182 As an alternative SIT data to evaluate the SIT distribution in the ESS, we used ~~To evaluate the~~
183 ~~reliability of the SIT values in the TOPAZ4 reanalysis data during the freezing season, we mainly~~
184 ~~used~~ the merged product of CryoSat-2 (CS2) and the Soil Moisture and Ocean Salinity (SMOS) SIT
185 products (hereafter, CS2SMOS) from 2011 to 2014 [Ricker et al. 2017], which were provided by

186 the online sea-ice data platform “meereisportal.de” ([For details, acknowledgement](#)) [Grosfeld et al.
187 2016]. These data are interpolated to 25-km resolution based on optimal interpolation and they are
188 available from October to April. In general, CS2 data have large uncertainty in the estimation of
189 SIT of <1 m, while the SMOS relative uncertainties are lowest for very thin ice. Thus, the merged
190 product is – to date – considered the best estimate of the [satellite-based](#) SIT distribution [in and](#)
191 [around the ESS](#)~~across the entire Arctic Ocean, including the ESS, although it was reported that~~
192 [there is potential negative bias in mixed first-year and multiyear ice regions such as the Beaufort](#)
193 [Sea \[Ricker et al. 2017\]](#).

194 For the melting season (May–July), there is no reliable estimate of SIT distribution in the ESS,
195 we therefore used only in situ SIT data of autonomous ice mass balance (IMB) buoys obtained
196 ~~between 26 March and 29 July 2014~~ near the ESS [Perovich et al., 2013]. [During 2011 to 2014,](#)
197 [total 4 buoys are available in a whole year including the melting season \(the period in each buoy is](#)
198 [listed in Table 1\)](#). To compare the two-dimensional SIT data with IMB buoy data, we re-gridded the
199 gridded SIT data along the IMB buoy trajectories. This comparison method is almost identical to
200 that adopted by Sato and Inoue [2017] who compared IMB buoy data with SIT data of the
201 NCEP-CFSR reanalysis. ~~– As a reference for SIC, we used daily mean SIC data derived from~~
202 ~~AMSR2 passive microwave radiometer sensors using the bootstrap algorithm [Comiso and Nishio,~~
203 ~~2008; JAXA, 2013]~~. [Before comparing the gridded SIT data with IMB buoy data in each grid point,](#)
204 [we reconstructed these SIT data on a 0.25° latitude–longitude grid by applying bilinear](#)
205 [interpolation. The temporal and horizontal resolutions of the observed and simulated SIT data are](#)
206 [summarized in Table 1.](#)

207 To examine the source of medium-range predictability in SIT distribution, we also used
208 ECMWF atmospheric forecast data on a 1.25° latitude–longitude grid from 2013 to 2016, derived
209 from the THORPEX Interactive Grand Global Ensemble through its data portal
210 (<http://tigge.ecmwf.int>). This dataset is very similar to the atmospheric forecast data used [infor](#) the

211 TOPAZ4 operational forecast system [Simonsen et al. 2017]. For the examination of atmospheric
212 forecast skill, we used 51 ensemble daily means of zonal and meridional wind speed at 10-m height
213 on the same days ~~as for~~ the TOPAZ4 forecast data at lead times of 0–10 day.

214 To evaluate the influence of sea ice condition on vessel speed in the ESS [including the Laptev](#)
215 [and Kara Seas](#), we used [the vessel speed data derived from](#) Automatic Identification System (AIS)
216 ~~data~~ from two tankers during their passage through the ESS on 4–26 July 2014, which were
217 provided by Shipfinder (<http://jp.shipfinder.com/>). [The temporal resolution is about 2 to 3 hours,](#)
218 [depending on the timing and relative location of the satellite track and the ground-based receiver](#)
219 [station of AIS signal](#). Their ice classes correspond to IA Super in the Finnish–Swedish Ice Class
220 Rules, and these vessels are capable of navigating sea ice regions in which SIT is up to 50–90 cm.
221 Both tankers were likely to be hindered considerably by ice conditions, even under escort by
222 Russian nuclear-powered ice-breakers; thus, these AIS data are considered suitable for a case study
223 of the influence of SIT on icebreaker speed.

224 225 **3 Comparisons between TOPAZ4 and other available SIT data**

226 Figure 1a shows the spatial distribution of [PIOMAS](#) ~~observed (CS2SMOS)~~ SIT in [July](#) ~~April~~
227 ~~(when SIT is maximum)~~ in the Arctic marginal seas of the Laptev Sea, ESS, and Chukchi ~~sea~~ [Sea](#).
228 The [PIOMAS sea ice observations](#) shows [the tongue-like distribution of SIT, characterized by](#)
229 [relatively thick ice \(>1.0 m\) extending from the North Pole to the ESS. Since in this region, sea ice](#)
230 [motion tends to be converging during winter \[Kimura et al. 2013\], the sea ice is likely to increase](#)
231 [the thickness by ridging and rafting and thus remains until the next early summer.](#) ~~the maximum~~
232 ~~thickness (>3 m) near Greenland, but relatively thick ice (~1.8 m) can also be found around the ESS.~~
233 These features are qualitatively simulated in the TOPAZ4 reanalysis data ([Fig. 1b](#)). ~~(Fig. 1b).~~ ~~The~~
234 ~~differences in SIT between the TOPAZ4 reanalysis and CS2SMOS data reveal remarkable negative~~
235 ~~bias (i.e., smaller than 0.8 m) in the TOPAZ4 reanalysis in the central Arctic Ocean (Fig. 1e);~~

236 ~~however, the magnitude of the negative bias is smaller in coastal areas such as the ESS.~~ The PCC of
237 the climatological SIT between TOPAZ4 and ~~PIOMAS~~CS2SMOS in the Arctic marginal seas
238 (~~70~~65°–80°N, ~~120~~80°E–160°W, shown in Fig. 1a) is larger than 0.9 from March to July. The ~~0.89~~
239 ~~in April, which is comparable with that between the PIOMAS output and CS2SMOS (Table~~
240 ~~2).~~PCCs of the climatological SIT between TOPAZ4 and CS2SMOS from March to April are 0.86
241 and 0.82, which are comparable to those of PIOMAS (Table 2).

242 From the difference map of the climatological SIT between TOPAZ4 reanalysis data and
243 PIOMAS output, the TOPAZ4 SIT is thicker near the coast with ~50 cm (Fig. 1c), although the SIT
244 in the offshore region is underestimated. These positive and negative biases compensate each other
245 and thus the mean bias of the TOPAZ4 SIT is 21 cm in July, which is smaller than in winter (Table
246 3). The seasonal reduction of the SIT bias in TOPAZ4 is also found in the comparison between the
247 TOPAZ4 and CS2SMOS (Table 3). In fact, a similar positive bias emerges in comparison with the
248 climatological SIT in CS2SMOS in April (Fig. 2). It should be noted that a larger positive bias in
249 TOPAZ4 is located solely in the region of the Beaufort Gyre, with about 50 cm excess thickness
250 (Fig. 1c and 2c). Since in this region, both SIT data sets show some negative bias relative to the
251 independent SIT estimates derived from U.S. submarine data [Schweiger et al. 2011] and airborne
252 electromagnetic induction (EM) thickness measurements [Ricker et al. 2017], this positive bias may
253 be partly related to the underestimation of PIOMAS and CS2SMOS SITs, themselves.

254 ~~The PCCs in other months are also comparable with those of the PIOMAS output. It should~~
255 ~~be noted that a larger positive bias in TOPAZ4 is located solely in the region of the Beaufort Gyre,~~
256 ~~with about 50 cm excess thickness (Fig. 1c). This positive bias is however consistent with the large~~
257 ~~underestimation of CS2SMOS SIT over the Beaufort Sea, which is related to the existence of~~
258 ~~heavily deformed ice [Ricker et al. 2017].~~

259 Figure ~~3~~2 shows the time series of daily mean SIT derived from PIOMAS and TOPAZ4
260 reanalysis and 7-days mean SIT derived from ~~CS2SMOS, TOPAZ4 reanalysis, and PIOMAS output,~~

261 averaged over the ESS (70°–80° N, 150°–180° E, shown in Fig. 1a). The TOPAZ4 SIT ~~data data~~ are
262 reasonably similar to the seasonal cycle of PIOMAS and CS2SMOS data data with maxima in
263 April–May and minima in October–November. In particular, the TOPAZ4 SIT is within the
264 standard deviation of PIOMAS SIT anomaly in each grid relative to the area-averaged value in
265 early summer (June-July). The monthly mean biases of TOPAZ4 SIT data relative to PIOMAS in
266 June and July are smaller than those in March to May (Table 3). It should be noted that the TOPAZ4
267 SIT data in 2011 are strongly underestimated in early summer. This might be related to the
268 persistence of the negative bias until 2010 [Xie et al., 2017].

269 In the freezing season, the TOPAZ4 SIT in the ESS tends to be thinner than the PIOMAS SIT,
270 and seems comparable to the CS2SMOS SIT. The monthly mean bias of TOPAZ4 SIT relative to
271 CS2SMOS SIT is -23 cm and 1 cm in March and April, respectively (Table 3). On the other hand,
272 we should pay attention to the possibility that the CS2SMOS SIT may be underestimated in this
273 region, because the CS2SMOS highly depends on the reliability of merging two SIT data, which are
274 CryoSat-2 and SMOS SIT products [Ricker et al. 2017]. To check the possibility that the CS2SMOS
275 SIT has a negative bias in this area, we briefly examined the ice type data which were used for the
276 determination of merged SIT products. In the period from 2011 to 2013, the uncertainty of
277 CS2SMOS SIT is out of range for that of PIOMAS, but the CS2SMOS SIT is comparable to that for
278 PIOMAS in 2014 when the sea ice is classified as multi-year ice (Fig. 3). This result implies that the
279 CS2SMOS SIT is underestimated in the ESS due to the large fraction of SMOS SIT products even
280 in the sea ice thicker than 1 m.

281 ~~;, although the TOPAZ4 SIT data at the beginning of 2011 are highly underestimated. This~~
282 ~~might be related to the persistence of the negative bias until 2010 [Xie et al., 2017].~~ Finally, we
283 compared the SIT data in TOPAZ4 with the in-situ observations available in and around the ESS.
284 Although the location of these buoy data are not fully delimited in the ESS focused in this study the
285 ESS on which we focused in this study, these data seem to be appropriate for our purpose, because

286 the range of the climatological SIT in these region is similar to that in the ESS (Fig. 1a). The direct
287 comparison between the TOPAZ4 and IMB shows that the mean bias and root mean square error of
288 TOPAZ4 is 8.3 cm and 30 cm, respectively (Fig. 4). In particular, the TOPAZ4 SIT data shows a
289 good correspondence with IMB buoy data in 2014, which is near the ESS in July (Fig. 1a and Table
290 1). These results support the reliability of TOPAZ4 SIT data in the ESS in early summer. Thus, at
291 least the overall spatial distribution of TOPAZ4-SIT in the ESS in the ESS is qualitatively simulated
292 in the TOPAZ4 and the inherent negative bias is suppressed in early summer, which is partly related
293 to the compensation by the positive bias near the shelf region of the ESS. ~~can be considered~~
294 ~~successful in simulating the seasonal cycles of CS2SMOS and IMB buoy data within the range of~~
295 ~~approximately ± 20 cm, which is lower than the negative bias found in the central Arctic Ocean. The~~
296 ~~errors in the central Arctic Ocean and Beaufort Sea are probably larger because they contain older~~
297 ~~multi-year ice for which the SIT errors have accumulated errors in sea ice drift and thermodynamics~~
298 ~~over longer times.~~

299

300

301 **4. Medium-range forecast skill of SIT distribution in the ESS**

302 In this section, we evaluate the prediction skill of SIT based on the PCCs between the analysis
303 and predicted data in the ESS. However, before this evaluation, we examine the mean fields and the
304 variability of the SIT and SIC distributions in early summer. Figure 54a presents the spatial
305 distribution of the climatological SIT and SIC in July, which shows that relatively thick sea ice (~ 1
306 m) covers 50%–70% of the ESS. Along the zone of the sea ice edge, the temporal standard
307 deviation of the daily mean SIT anomaly is relatively large with the maximum value of 0.6 m in the
308 coastal region (Fig. 54b) and the area-averaged value is maximum in July–August (Fig. 54c). Since
309 the SIT reduction rate in the ESS is strongest in these months (Fig. 54c) and the storm activity is
310 prevalent for periods of several days [Orsolini and Sorteberg, 2009], it is likely that dynamical and

311 thermodynamically-induced SIT variations are large. Note that the RMS of the SIC anomaly
312 averaged over the ESS also shows a similar seasonal cycle (not shown). Thus, it is meaningful to
313 examine the medium-range predictability of early summer SIT distribution in the ESS.

314 Figure [6.5a](#) shows the seasonal dependency of PCC between the predicted and analyzed SIT at
315 lead times of 0–9 days. We found that the overall prediction skill is relatively low in [warm season](#)
316 [\(June–September\)](#) ~~July~~ with a larger spread compared with the cold season [\(October–January–May\)](#).
317 ~~This result is roughly, which is~~ consistent with the larger variance of the SIT anomaly in [the warm](#)
318 [season in](#) the ESS (Fig. [5.4c](#)). [A large portion of the prediction skill at the lead times of 0–3 days can](#)
319 [be explained by the persistency effect based on the initial SIT \(Fig. 6b\). The contribution of the](#)
320 [operational model on the forecast skill is less than 5% at shorter timescale \(<3 days\) \(Fig. 6c\), but](#)
321 [the contribution of the operational model gradually increases at longer lead times except in May and](#)
322 [October. In July, the contribution of the operational model on the prediction skill reaches ~15% at 7](#)
323 [day lead time. These results indicate that the operational model substantially improves the](#)
324 [medium-range prediction skill of the SIT distribution in summer.](#)

325 Figure 7a shows the PCC of SIT distribution averaged in early summer (June–July). ~~In early~~
326 ~~summer (June–July),~~ [The SIT distribution is predicted skillfully for a lead time of up to 3 days \(Fig.](#)
327 [7a](#) ~~Fig. 6~~); however, the prediction skill decreases abruptly at a lead time of 4 days, in which the
328 standard deviation is also relatively large. [Such an abrupt reduction of the prediction skill and the](#)
329 [enhanced standard deviation are also found in May and September, although the absolute values of](#)
330 [the reduction rates are smaller than in July. Since the influence of sea ice melt is small in these](#)
331 [months \(Fig. 5c\), the abrupt reduction of early summer SIT prediction skill might be attributable to](#)
332 [dynamical advection of sea ice.](#) ~~Since such an abrupt reduction of the prediction skill is also found in~~
333 ~~May and October (Fig. 5), when the influence of sea ice melt is quite small (Fig. 4c), the abrupt~~
334 ~~reduction of early summer SIT prediction skill might be attributable to dynamical advection of sea~~
335 ~~ice.~~

336 To examine the influence of dynamical processes on the prediction skill of early summer SIT
337 distribution, we consider the prediction skill of sea ice velocities and surface wind velocities. The
338 prediction skill of sea ice velocity stays on a high level (≥ 0.8) with small spread for a lead time of
339 up to 3 days, but decreases down to 0.6–0.7 for a lead time of 4 days (Fig. 7b7a). The early summer
340 prediction skill of surface wind speed also shows the same abrupt decrease at a lead time of 4 days,
341 and the rate of decrease of prediction skill is larger in meridional direction (Fig. 77cb). Since the
342 SIT distribution has a tongue-like distribution~~zonally homogeneous pattern~~ (Fig. 54a), it is
343 suggested that the meridional component of SIT advection is sensitive to the sea ice transport in
344 ice-edges, which influences the SIT distribution in the ESS. These results confirm that the
345 prediction skills of the sea ice velocities are strongly related to those of surface wind speeds in the
346 ESS.

347 Figure 88 shows the temporal evolutions of SIT and ice velocity for analysis and a forecast
348 bulletin starting from 2nd July 2015, which is a typical case of the abrupt decrease in the prediction
349 skill of SIT as well as sea ice velocities for a lead time of 4 days (Fig. 88; lower panel). For lead
350 times of +0 (2 July) to +2 days (4 July), the spatial distributions of SIT and ice velocity are
351 predicted skillfully with only small differences between them (Fig. 88; right panels). At a lead time
352 of +4 days (6 July), the analyzed sea ice velocity is directed northwestward in the ESS, which is
353 related to the cyclonic circulation over the Novosibirsk Islands; however, the predicted sea ice
354 velocity is directed southwestward. At a lead time of +6 days, the predicted and analyzed sea ice
355 velocities are largely~~completely~~ unrelated. The resultant onshore~~southward~~ anomaly of sea ice
356 velocity leads to positive and negative anomalies in SIT in the coastal and offshore regions,
357 respectively. We also examined the time evolutions of the surface wind velocities in the
358 atmospheric forecast data, and found them very similar to the sea ice velocity fields (not shown).
359 These results indicate that the abrupt reduction of the prediction skill of early summer SIT in the

360 ESS is related to a deficiency [in the prediction of Arctic cyclone formation](#) ~~at predicting Arctic~~
 361 ~~eyelone~~.

362 Further, we examine diagnostically the ice drift speed and direction based on a classical
 363 free-drift theory [Leppäranta, 2005], using the sea ice speed of TOPAZ4 reanalysis data and ERA
 364 interim atmospheric wind data in July 2011– 2014. The general solution of sea ice speed (u) can be
 365 described as complex numbers:

$$366 \quad u = \alpha e^{-i\theta} U_a + U_{wg} \quad (2)$$

367 where U_a , and U_{wg} are the wind speed and geostrophic water velocities, respectively. The terms α
 368 and θ are the wind factor and the deviation angle of ice motion from the surface wind, respectively,
 369 where a positive angle is in counterclockwise direction. If we neglect the geostrophic water velocity
 370 U_{wg} , the wind factor and deviation angle can be obtained in the following form:

$$371 \quad \alpha^4 + 2 \sin \theta_w RNa\alpha^3 + R^2 Na^2 \alpha^2 - Na^4 = 0, \quad (3)$$

$$372 \quad \theta = \arctan \left(\tan \theta_w + \frac{RNa}{\alpha \cos \theta_w} \right) - \theta_a, \quad (4)$$

373 where θ_w and θ_a are the boundary layer turning angles of water and air, respectively. The turning
 374 angle θ is the angle between the vectors of the ice–water stress and the sea ice motion, which is a
 375 consequence of the viscous effect within the ocean boundary layer. The Nansen number Na is
 376 defined by $\sqrt{\rho_a C_a / \rho_w C_w}$, where ρ_a and ρ_w represent the density of air and water, respectively, and
 377 C_a and C_w are air and water drag coefficients, respectively. The Rossby number R is defined by
 378 $(\rho h_{ice} f) / (\rho_w C_w Na |U_a|)$, where ρ is the ice density, f is the Coriolis parameter, and $|U_a|$ is the speed
 379 of the surface wind. To calculate the wind factor α and the deviation angle θ under a given surface
 380 wind speed, we used constant parameters of $C_a = 1.2 \times 10^{-3}$, $C_w = 5 \times 10^{-3}$, $\rho_a = 1.3 \text{ kg m}^{-3}$, $\rho_w =$
 381 1026 kg m^{-3} , $\rho = 910 \text{ kg m}^{-3}$, $f = 1.3 \times 10^{-4} \text{ s}^{-1}$, and $\theta_w = 20^\circ$, which are values typical of the Arctic

382 Ocean [McPhee, 2012]. The value of α was calculated numerically from a 4th-order polynomial (Eq.
383 (3)).

384 On a first order approximation, the daily mean sea ice speed is linearly proportional to the
385 surface wind speed (10-m height) averaged over a part of the ESS (Fig. 99a). The correlation
386 between them is 0.96, which is significant at the 99% confidence level, based on the Monte Carlo
387 simulation [Kaplan and Glass, 1995]. The regression coefficient of ice speed onto the 10-m wind
388 speed is 0.022, which is consistent with the well-known 2% relationship between the speed of ice
389 and the surface wind speed [Thorndike and Colony, 1982]. The number of the TOPAZ4 ice speed
390 data within $\pm 20\%$ of the theoretical value is 79 days, which accounts for 63% of the total analyzed
391 period. Note that the observed regression coefficient is somewhat larger than the theoretical value
392 (0.018) averaged over the range of surface wind speed of 2–10 m s^{-1} calculated from Eq. (2). Since
393 the classical free drift theory [Leppäranta, 2005] neglects both the Ekman layer velocity and the
394 ocean geostrophic velocity, the absence of an ice-ocean boundary layer is likely to underestimate
395 the wind-induced ice velocity [Park and Stewart, 2016]. The deviation angle of sea ice motion in
396 TOPAZ4 is estimated as 20° – 40° under a wind condition $> 5 \text{ m s}^{-1}$, but it gradually increases to
397 40° – 70° under weaker wind conditions of $< 5 \text{ m s}^{-1}$ (Fig. 99b). The decrease of the deviation
398 angle as the surface wind strengthens is also consistent with earlier studies [Thorndike and Colony,
399 1982]. These observed deviation angles are comparable with their theoretical values calculated
400 using Eq. (4). The finding that the estimated values of the wind factor and the deviation angle are
401 approximately within the range of typical surface wind parameters (i.e., 2% for the wind factor and
402 30° for the deviation angle) in the Arctic Ocean confirms that sea ice velocity in the ESS is
403 controlled predominantly by wind stress drag: thus, the influence of ocean currents is not essential.

404 It is interesting that the prediction skill of SIT in early summer remains ~ 0.9 for the PCC core
405 at the lead times longer than 4 days ~~at high level after the lead time of 4 days~~ (Fig. 76a), despite the
406 poorer prediction skill of sea ice velocity (Fig. 7b7a). This suggests that the SIT prediction skill

407 after a lead time of 4 days is not [strongly](#) attributed to the dynamical process but rather the
408 thermodynamic process (i.e., the melting process of sea ice). To evaluate the effect of sea ice
409 melting on SIT prediction skill, we roughly estimated the thermodynamic SIT change based on a
410 simple sea ice melting model, as follows:

$$411 \quad h^p(t) = h^a(t_0) + \Delta t \times d\bar{h} / dt \quad (5)$$

412 where h^p is the predicted thermodynamic SIT change, h^a is the initial condition, which is
413 derived from the analysis SIT, and $d\bar{h} / dt$ is the rate of reduction of SIT due to sea ice melting. It
414 is known that the summertime surface heat flux in the Pacific sector of the Arctic Ocean is
415 dominated by the shortwave radiation flux [Perovich et al. 2007; Steele et al. 2008]. Recently, the
416 seasonal evolution of sea ice retreat in early summer has been found to be explained well by a
417 simplified ice–ocean coupled model, in which shortwave radiation is assumed constant [Kashiwase
418 et al. 2017]. Therefore, as the melting rate of the SIT in each year, we used the reduction rate of SIT
419 calculated from the climatological analysis SIT data during 2013–2016, which is likely to reflect the
420 typical thermodynamic melting rate in recent years and the SIT change due to transient sea ice
421 advection seems to be negligible. Here, we also evaluate the prediction skill of the persistency in the
422 initial SIT in the ESS (first term of the RHS in Eq. (5)).

423 Figure [10+0](#) shows the prediction skills of early summer SIT [distribution in the ESS based on](#)
424 ~~in~~ the simple sea ice melting and persistency models. The prediction skill of the simple melting
425 model, which is lower than the full physics model, is very similar to that of the persistency model
426 up to 3 days. However, the prediction skill of the simple melting model is comparable with that of
427 the full physics model after a lead time of 4 days, which is higher than that of persistency. Figure
428 [11+1](#) shows the temporal evolutions of SIT difference between the forecast and analysis data in each
429 prediction model in the period 2–9 July 2015. From the lower panel of Fig. [11+1](#), we found that the
430 prediction skill of the full physics model is higher than the simple melting and persistency models

431 for lead times of 0–5 days, but comparable with the prediction skill of the simple melting model at
432 longer lead times (> 6 days). In the SIT difference map of the full-physics model minus the
433 operational analysis, a positive anomaly (i.e., overestimation of SIT), is evident along the sea ice
434 edge at a lead time of 4 days, and then gradually increases until a lead time of 8 days. For the case
435 of the simple melting model, a similar positive anomaly emerges at a lead time of 4 days, but the
436 positive anomaly appears stationary along the coastal region, compared to the full physics model.
437 The persistency model overestimates SIT over the entire region during the prediction. These results
438 support the idea that the melting process is important in the prediction of early summer SIT over
439 longer timescales. ~~Looking back at the seasonal dependency of SIT prediction skill (Fig. 5), the loss
440 of prediction skills past the 4th day in December–February appear larger than in June–August. The
441 difference in prediction skill between lead times of 4 day and 9 day, averaged in January–February,
442 is 0.05, which is somewhat larger than in June–July (0.03). This result implies that the wintertime
443 SIT prediction skill without any thermodynamic melting process is largely controlled by the weak
444 skill of atmospheric prediction, and thus indirectly supports the assertion that the extension of the
445 skillful prediction of early summer SIT is attributable to the thermodynamic melting process.~~

446

447 **5. Case study of ice-blocked incident in the ESS in July 2014**

448 In the perspective of operational application of the TOPAZ4 sea ice data to the maritime
449 navigation of the NSR, we briefly examine the relationship between the sea ice conditions and AIS
450 vessel speed data for the case of an ice-blocking incident involving two vessels, based on the
451 TOPAZ4 reanalysis data. Figure ~~12~~¹³ shows the vessel tracks during July 4–30 2014, when the two
452 vessels became blocked in the ESS for about one week. During this period, SIT in excess of 100 cm
453 is found in the ESS with the maximum thickness of 150 cm. A joint statistical analysis of the daily
454 mean SIT in the TOPAZ4 reanalysis and the vessel speed along the route indicates that vessel speed
455 is significantly anticorrelated with SIT (~~-0.56~~^{-0.80}) during the entire passage (Fig. ~~13~~^{14aa}),

456 significant at the ~~99~~95 % confidence level based on a Monte Carlo technique [Kaplan and Glass,
457 1995]. We also examined the corresponding SIC data in TOPAZ4 reanalysis data, but the
458 correlation between the vessel speed and SIC is -0.41 (Fig. 13b), which is insignificant at 99%
459 confidence level. The scatter plots for SIC indicates that the SIC value is partly insensitive to the
460 vessel speed higher than 5 knot. Thus, these results suggest that the vessel speed was influenced by
461 sea ice stress due to SIT and indirectly supports the reliability of the daily mean SIT of the TOPAZ4
462 reanalysis data in the ESS in early summer.~~The correlation between the SIC and vessel speed is also~~
463 ~~significant ($r = -0.77$), although the absolute value of the correlation coefficient is lower than for SIT.~~
464 ~~This result suggests that vessel speed was influenced by sea ice stress due to SIT and indirectly~~
465 ~~supports the reliability of the daily mean SIT of the TOPAZ4 reanalysis data in the ESS in early~~
466 ~~summer.~~

467

468 **6. Summary and discussion**

469 In this study, the medium-range forecast skill of early summer SIT distribution in the ESS was
470 evaluated using the TOPAZ4 data assimilation system. Comparisons between the operational model,
471 observed, ~~observed, operational model,~~ and TOPAZ4 reanalysis SIT data showed that the TOPAZ4
472 reanalysis qualitatively reproduces the tongue-like distribution of SIT in the ESS in early summer,
473 and its seasonal variation (maximum in April–May and minimum in October–November) including
474 the rates of advance and melting of sea ice in the ESS). Although in this region, the inherent
475 negative bias of SIT in TOPAZ4 is relatively large in March to May, the bias is reduced in early
476 summer (June–July) within $\sim \pm 20$ cm due to the excess of SIT along the coastal region in the ESS.
477 The TOPAZ4 SIT data also shows a good correspondence with IMB buoy data in and around the
478 ESS with the mean bias of ~ 9 cm and the root mean square error of ~ 30 cm. ~~observed seasonal~~
479 ~~variation (maximum in April–May and minimum in October–November) including the rates of~~
480 ~~advance and melting of sea ice in the ESS. Earlier studies have identified that the SIT of the~~

481 ~~TOPAZ4 reanalysis data is underestimated, even in the ESS, but the negative bias relative to the in~~
482 ~~situ and satellite observations was about 20 cm from winter to summer, which is smaller than~~
483 ~~another reliable hindcast model output (PIOMAS).~~ Thus, the TOPAZ4 SIT data could be considered
484 reliable estimates for the ESS even in the absence of satellite observations in summer.

485 For the positive bias of the SIT in TOPAZ4 along the coastal region of the ESS, there is a
486 possibility that the SIT estimates (PIOMAS and CS2SMOS) used for the comparison are
487 themselves underestimated. Schweiger et al. [2011] pointed out that the SIT of PIOMAS is
488 underestimated by -17cm in the basin area of the Arctic Ocean including the Beaufort Sea where the
489 heavy deformed sea ice formation occurs. Also, it was reported that the CS2SMOS SIT data tend to
490 underestimate SIT in regions where multi-year ice and first-year ice are formed, due to the relative
491 accuracy of CryoSat-2 and SMOS and the merging algorithm [Ricker et al. 2017]. Since in the ESS,
492 sea ice motion is strongly converging during winter [Kimura et al. 2013], there is a possibility that
493 the sea ice in the ESS is also heavily deformed to form sea ice thicker than 1 m along the coastal
494 region. In fact, our analysis based on the AIS data suggests that SIT in excess of 100 cm is found
495 near the coast of the ESS. Thus, for a precise evaluation of the SIT distribution in the ESS, the
496 further improvement of ice-type as well as denser in-situ SIT measurements are needed.

497 The prediction skill of the SIT distribution in the TOPAZ4 forecast system was examined in
498 the ESS using a pattern correlation analysis. Although the prediction skill was relatively lower in
499 early summer (June–July) with a large spread, the SIT distribution was predicted skillfully for a
500 lead time of up to 3 days, and the prediction skill drops abruptly after the 4th day. A similar change
501 in prediction skill was also found for sea ice velocity and surface wind speed over the ESS.
502 Diagnostic analysis of the sea ice velocity variability revealed that the early summer ice speed and
503 direction over the EES could be explained well by the free-drift mechanism with a wind factor of
504 2.2 % and a deviation angle of 30°–50°. ~~Their~~There results suggested that the large reduction of
505 prediction skill could be attributed to the process of dynamical advection of sea ice; thus, the

506 prediction of early summer SIT distribution will depend on precise prediction of the surface wind.
507 Our comprehensive analysis supports an earlier study that suggested the dynamical processes have
508 an essential role in the prediction skill of sea ice distribution on short timescales [Ono et al., 2016].

509 The time evolution of SIT and the related ice velocity relates the large difference between the
510 forecast and analysis data at a lead time of 4 days to the low forecast skills for an Arctic cyclone
511 event. Jung and Matsueda [2017] highlighted that large-scale atmospheric fluctuations in the Arctic
512 region in winter are predicted skillfully for lead times of up to 5 days in the operational forecast
513 system, which is very similar to the prediction skill in mid-latitude regions. However, Yamagami et
514 al. [2018] reported that the skillful prediction of Arctic cyclones generated in summer is limited to 4
515 days, which is shorter than the case for the mid-latitudes [Froude, 2010]. As this area is located near
516 the transit zone of summertime storm tracks generated over Eurasia [Serreze and Barry, 1988], the
517 predictability of Arctic cyclones could be an important factor in the determination of the lead time
518 of surface wind speed and thus, of the SIT distribution in the ESS. The low prediction skill of the
519 meridional wind and ice speed suggested that the meridional component of sea ice advection
520 contributes substantially to the SIT distribution in the ESS. Since it was reported that additional
521 radiosonde observations over the Arctic Ocean have considerable impact on the prediction skill in
522 synoptic-scale fluctuations [Inoue et al., 2015; Yamazaki et al., 2015], additional radiosonde
523 observations acquired over the Arctic Ocean could lead to further extension of the lead time for
524 medium-range forecast skill of SIT distribution.

525 ~~It is interesting that the prediction skill of early summer SIT remains at a high level after a lead~~
526 ~~time longer than 4 days in spite of the poor prediction skill of the sea ice velocity and surface wind~~
527 ~~fields.~~ Based on sensitivity experiments using a simple melting and a persistency model, it was
528 found that the longer timescale prediction of SIT in early summer could be attributed to the
529 thermodynamic melting process. As the shortwave radiation flux is maximum in early summer
530 (June–July), the change of SIT due to the advection in relation to synoptic-scale atmospheric

531 fluctuations is likely to be smaller than the thermodynamic SIT reduction along the sea ice edge.
532 Although the recognition of the importance of the thermodynamic melting process on sea ice
533 prediction on seasonal timescales has been pointed out by earlier studies [Kimura et al. 2013~~2~~;
534 Bushuk et al. 2017; Kashiwase et al. 2017], our study clarified that the influence has a substantial
535 role on the medium-range forecast of early summer SIT distribution. Thus, the influence of sea ice
536 advection on early summer sea ice prediction is limited to a lead time of 4–5 days, but is dominated
537 by the thermodynamic melting process in later stage of the lead times. In other words, the SIT
538 prediction skill in early summer is not necessarily worse at the longer timescale. It is noteworthy
539 that the dynamical process is not unimportant for the long-term prediction in the SIT distribution in
540 early summer, because the skillful prediction skill at a lead time of 3 days is important as the initial
541 conditions for the melting process dominated for a lead time longer than 4 days. Thus, it is
542 concluded that the atmospheric prediction skill for a lead time of up to 3 days contributes to the
543 short and medium-range prediction skill of the SIT distribution in early summer.

544 In view of the operational application of the TOPAZ4 sea ice data to the navigation in NSR,
545 this study found that during an ice-blocking event that affected two tankers in the ESS in July 2014,
546 significant SIT (~150 cm) was simulated over the ESS by TOPAZ4. Given that the SIT is found to
547 be underestimated by 20 cm in TOPAZ4, the true SIT is expected to be above 150 cm. Statistical
548 analysis suggested that vessel speed was ~~significantly~~ ~~highly~~ anticorrelated with the daily mean SIT
549 variations (~~-0.56~~~~0.80~~) rather than the SIC (~~-0.41~~~~0.77~~). This result demonstrated the reliability of
550 the early summer SIT distribution in the TOPAZ4 reanalysis data and its high potential for
551 operational use in support of maritime navigation of the NSR. However, this result was only based
552 on a case study of two ships in July 2014. To clarify the determinant factor on vessel speed,
553 comprehensive statistical analysis will be needed based on the speed data of different types of
554 vessel.

555 Future projections for storm track activity (intensity and number) under the scenario of Arctic
556 climate change have been addressed by several researchers. For example, based on control
557 experiments using climate models, Bengtsson et al. [2006] found that summertime storm activity is
558 expected to increase. Orsolini and Sorteberg [2009] found that the number of storms, particularly
559 along the Eurasian Arctic coast, could increase in the future, because of the local enhancement of
560 the meridional temperature gradient between the Arctic Ocean and the warmed Eurasian continent.
561 Nishii et al. [2015] supported that their findings based on analyses using the [CMIP3 and CMIP5](#)
562 [global climate model simulations](#)~~Coupled Model Intercomparison Project (CMIP) 3 and 5~~,
563 although they highlighted that the CMIP projections had considerable uncertainty. Thus, further
564 investigations of the formation and the development mechanisms of summertime Arctic cyclones
565 are needed for the improvement of the prediction skill of atmospheric wind conditions, which are
566 responsible for the forecast skill of early summer sea ice distribution over 4 days.
567

568 **Acknowledgements**

569 The AMSR2 brightness temperatures and products data were provided by the Japan Aerospace
570 Exploration Agency (JAXA). The dataset of AMSR2 SIT and SIC was archived and provided by the
571 Arctic Data archive System (ADS), which was developed by the National Institute of Polar
572 Research (NIPR). The merging of CryoSat-2 und SMOS data was funded by the ESA project
573 SMOS+ Sea Ice (4000101476/10/NL/CT and 4000112022/14/I-AM) and data from 2010 to 2014
574 were obtained from <http://www.meereisportal.de> (Grant No.: REKLIM-2013-04). The ECMWF
575 atmospheric forecast data were provided by the ECMWF TIGGE portal site via the TIGGE medium
576 of the University of Tsukuba (<http://gpvjma.ccs.hpcc.jp/TIGGE/>). The TOPAZ4 forecast data were
577 analyzed using the Pan-Okhotsk Information System of ILTS. This work was ~~supported by~~ ~~funded~~
578 ~~by the~~ Arctic Challenge for Sustainability (ArCS) project of the Ministry of Education, Culture,
579 Sports, Science and Technology in Japan, and JSPS KAKENHI Grant Numbers JP17KK0014,
580 JP18H0374. We thank James Buxton MSc from Edanz Group (www.edanzediting.com/ac) for
581 correcting a draft of this manuscript.

582

583 **References**

- 584 Barnett T. P., & Schlesinger M. E. 1987. Detecting changes in global climate induced by
585 greenhouse gases. *J. Geophys. Res.* 92, 14772–14780, doi:10.1029/JD092iD12p14772.
- 586 Bengtsson L., Hodges K.I., & Roeckner E. 2006. Storm Tracks and Climate Change. *J. Climate* 19,
587 3518–3543, <https://doi.org/10.1175/JCLI3815.1>.
- 588 Blanchard-Wrigglesworth E. & Bitz, C. M. 2014. Characteristics of Arctic Sea-Ice Thickness
589 Variability in GCMs. *J. Climate* 27, 8244–8258.
- 590 Bushuk M., Msadek R., Winton M., Vecchi G. A., Gudgel R., Rosati A., & Yang X. 2017. Skillful
591 regional prediction of Arctic sea ice on seasonal timescales. *Geophys. Res. Lett.* 44,
592 doi:10.1002/2017GL073155.
- 593 Cavalieri D. J. & Parkinson C. L. 2008. Arctic sea ice variability and trends, 1979–2006. *J.*
594 *Geophys. Res.* 113, C07003, doi:10.1029/2007JC004558.
- 595 Chen Z., Liu J., Song M., Yang Q., & Xu S. 2017. Impacts of Assimilating Satellite Sea Ice
596 Concentration and Thickness on Arctic Sea Ice Prediction in the NCEP Climate Forecast
597 System. *J. Climate* 30, 8429–8446.
- 598 Collow T., Wang W., Kumar A., & Zhang J. 2015. Improving Arctic Sea Ice Prediction Using
599 PIOMAS Initial Sea Ice Thickness in a Coupled Ocean–Atmosphere Model. *Mon. Wea. Rev.*
600 143, 4618–4630, doi: 10.1175/MWR-D-15-0097.1.
- 601 Comiso J. C. 2012. Large Decadal Decline of the Arctic Multiyear Ice Cover. *J. Climate* 25, 1176–
602 1193, <https://doi.org/10.1175/JCLI-D-11-00113.1>.
- 603 Dee D. P. et al. 2011. The ERA-Interim reanalysis: configuration and performance of the data
604 assimilation system. *Q.J.R. Meteorol. Soc.* 137, 553–597. doi: 10.1002/qj.828.
- 605 Eguíluz V. M., Fernández-Gracia J., Irigoien X., & Duarte C. M. 2016. A quantitative assessment
606 of Arctic shipping in 2010–2014. *Sci. Rep.* 6, 30682, doi:10.1038/srep30682.
- 607 Fichetfet T., & Maqueda M. A. M. 1997. Sensitivity of a global sea ice model to the treatment of ice

608 thermodynamics and dynamics. *J. Geophys. Res.* 102, 12609–12646, doi:10.1029/97JC00480.

609 Froude L. S. R. 2010. TIGGE: Comparison of the prediction of Northern Hemisphere extratropical
610 cyclones by different ensemble prediction systems. *Weather and Forecasting* 25, 819–836.
611 <https://doi.org/10.1175/2010WAF2222326.1>.

612 Grosfeld K., Treffeisen R., Asseng J., Bartsch A., Bräuer B., Fritsch B., Gerdes R., Hendricks S.,
613 Hiller W., Heygster G., Krumpen T., Lemke P., Melsheimer C., Nicolaus M., Ricker R., &
614 Weigelt M. 2016. Online sea-ice knowledge and data platform <www.meereisportal.de>,
615 Polarforschung, Bremerhaven, Alfred Wegener Institute for Polar and Marine Research &
616 German Society of Polar Research 85, 143-155, doi:10.2312/polfor.2016.011.

617 Holland M. M., Bailey, D. A. & Vavrus, S. 2011. Inherent sea ice predictability in the rapidly
618 changing Arctic environment of the Community Climate System Model, version 3. *Clim. Dyn.*
619 36, 1239–1253, doi:10.1007/s00382-010-0792-4.

620 Honda M., Inoue J., & Yamane S. 2009. Influence of low Arctic sea-ice minima on anomalously
621 cold Eurasian winters. *Geophys. Res. Lett.* 36, L08707, doi:10.1029/2008GL037079.

622 Hunke E. & Dukowicz J. 1997. An Elastic–Viscous–Plastic Model for Sea Ice Dynamics. *J. Phys.*
623 *Oceanogr.* 27, 1849–1867.

624 Inoue J., Hori M., & Takaya K. 2012. The role of Barents sea ice in the wintertime cyclone track
625 and emergence of a Warm-Arctic Cold Siberian anomaly. *J. Climate* 25, 2561-2568.

626 Inoue J., Yamazaki A., Ono J., Dethloff K., Maturilli M., Neuber R., Edwards P., & Yamaguchi H.
627 2015. Additional Arctic observations improve weather and sea-ice forecasts for the Northern
628 Sea Route. *Sci. Rep.* 5, 16868, doi:10.1038/srep1686.

629 JAXA 2013. Descriptions of GCOM-W1 AMSR2 Level 1R and Level 2 Algorithms, Rev. A.

630 Jung, T. & Matsueda, M. 2016. Verification of global numerical weather forecasting systems in
631 polar regions using TIGGE data. *Q.J.R. Meteorol. Soc.* 142: 574–582. doi: 10.1002/qj.2437.

632 Kaplan, D. & Glass L. 1995. *Understanding nonlinear dynamics*, Springer-Verlag, New York, pp.

633 420.

634 Kara A., Rochford P., & Hurlburt H. 2000. Efficient and Accurate Bulk Parameterizations of Air–
635 Sea Fluxes for Use in General Circulation Models. *J. Atmos. Oceanic Technol.* 17, 1421–1438.

636 Kashiwase H., Ohshima K. I., Nihashi S., & Eicken H. 2017. Evidence for ice-ocean albedo
637 feedback in the Arctic Ocean shifting to a seasonal ice zone. *Sci. Rep.* 7, 8170,
638 doi:10.1038/s41598-017-08467-z.

639 Kimura N., Nishimura A., Tanaka Y., & Yamaguchi H. 2013. Influence of winter sea-ice motion on
640 summer ice cover in the Arctic. *Polar Research* 1751-8369,
641 doi:http://dx.doi.org/10.3402/polar.v32i0.20193.

642 Large W.G. & Pond S. 1981. Open Ocean Momentum Flux Measurements in Moderate to Strong
643 Winds. *J. Phys. Oceanogr.* 11, 324–336.

644 Laxon S. W., Giles K. A., Ridout A. L., Wingham D. J., Willatt R., Cullen R., Kwok R., Schweiger
645 A., Zhang J., Haas C., Hendricks S., Krishfield R., Kurtz N., Farrell S. & Davidson M. 2013.
646 CryoSat-2 estimates of Arctic sea ice thickness and volume, *Geophys. Res. Lett.* 40, 732–737.

647 Leppäranta M. 2005. *The Drift of Sea Ice*. Springer-Verlang, 266 pp.

648 Lisæter K. A., Rosanova J., & Evensen G. 2003. Assimilation of ice concentration in a coupled
649 ice-ocean model, using the Ensemble Kalman filter. *Ocean Dynamics* 53, 368–388.
650 <http://doi.org/10.1007/s10236-003-0049-4>.

651 Lindsay R.W. & Zhang J. 2006. Arctic Ocean Ice Thickness: Modes of Variability and the Best
652 Locations from Which to Monitor Them. *J. Phys. Oceanogr.* 36, 496–506,
653 <https://doi.org/10.1175/JPO2861.1>.

654 Lindsay R. W., Zhang J., Schweiger A. J., & Steele M. A. 2008. Seasonal predictions of ice extent
655 in the Arctic Ocean. *J. Geophys. Res.* 113, C02023, doi:10.1029/2007JC004259.

656 McPhee M. G. 2012. Advances in understanding ice-ocean stress during and since AIDJEX. *Cold
657 Reg. Sci. Technol.* 76, 24-36.

- 658 Melia N., Haines K., & Hawkins E. 2015. Improved Arctic sea ice thickness projections using
659 bias-corrected CMIP5 simulations. *The Cryosphere* 9, 2237-2251,
660 doi:10.5194/tc-9-2237-2015.
- 661 Melia N., Haines K., & Hawkins E. 2016. Sea ice decline and 21st century trans-Arctic shipping
662 routes. *Geophys. Res. Lett.* 43, 9720–9728, doi:10.1002/2016GL069315.
- 663 Melia N., Haines K., Hawkins E., & Day J. J. 2017. Towards seasonal Arctic shipping route
664 predictions. *Env. Res. Lett.* 12, 084005.
- 665 Mori M., Watanabe M., Shiogama H., Inoue J., & Kimoto M. 2014. Robust Arctic sea-ice influence
666 on the frequent Eurasian cold winters in past decades. *Nat. Geosci.*, 7, 869–873.
- 667 ~~Nakanowatari T., Sato K., & Inoue J. 2014. Predictability of the Barents Sea Ice in Early Winter:
668 Remote Effects of Oceanic and Atmospheric Thermal Conditions from the North Atlantic. *J.*
669 *Climate* 27, 8884–8901, doi: 10.1175/JCLI-D-14-00125.1.~~
- 670 Nishii K., Nakamura H., Orsolini Y. J. 2015. Arctic summer storm track in CMIP3/5 climate
671 models. *Clim. Dyn.*, 44, 1311, <https://doi.org/10.1007/s00382-014-2229-y>.
- 672 Ono J., Inoue J., Yamazaki A., Dethloff K., & Yamaguchi H. 2016. The impact of radiosonde data
673 on forecasting sea-ice distribution along the Northern Sea Route during an extremely
674 developed cyclone. *J. Adv. Model Earth Syst.* 8, 292-303, doi:10.1002/2015MS000552.
- 675 Orsolini Y. J. & Sorteberg A. 2009. Projected changes in Eurasian and Arctic summer cyclones
676 under global warming in the Bergen climate model. *Atmos. Oceanic Sci. Lett.* 2, 62-67.
- 677 Overland J. E., Francis J. A., Hall R., Hanna E., Kim S.-J., & Vihma T. 2015. The melting Arctic
678 and mid-latitude weather patterns: Are they connected? *J. Climate*, 28, 7917-7932,
679 doi:10.1175/JCLI-D-14-00822.1.
- 680 Park H.-S. & Stewart A. L. 2016. An analytical model for wind-driven Arctic summer sea ice drift,
681 *The Cryosphere*, 10, 227–244.
- 682 Pastusiak T. 2016. *The Northern sea route as a shipping lane*. Springer, Switzerland, p. 219.

- 683 Perovich D. K., Light B., Eicken H., Jones K. F., Runcimen K., & Nghiem S. V. 2007. Increasing
684 solar heating of the Arctic Ocean and adjacent seas, 1979–2005: Attribution and the role of
685 ice-albedo feedback. *Geophys. Res. Lett.* 34, L19505, doi:10.1029/2007GL031480.
- 686 Perovich D., Richter-Menge J., Elder B., Arbetter T., Claffey K., & Polashenski C. 2013. Observing
687 and understanding climate change: Monitoring the mass balance, motion, and thickness of
688 Arctic sea ice. Cold Regions Research and Engineering Laboratory.
689 <http://www.imb-crrel-dartmouth.org/imb.creel>.
- 690 Persson A. 2011. User guide to ECMWF forecast products ver. 1.2, October 2011, ECMWF,
691 Reading, pp. 121.
- 692 Petoukhov V., & Semenov V. A. 2010. A link between reduced Barents-Kara sea ice and cold
693 winter extremes over northern continents. *J. Geophys. Res.* 115, D21111,
694 doi:10.1029/2009JD013568.
- 695 Ricker R., Hendricks S., Kaleschke L., Tian-Kunze X., King J., & Haas C. 2017. A weekly Arctic
696 sea-ice thickness data record from merged CryoSat-2 and SMOS satellite data. *The Cryosphere*
697 11, 1607-1623, <https://doi.org/10.5194/tc-11-1607-2017>.
- 698 Sakov P., & Oke P. R. 2008. A deterministic formulation of the ensemble Kalman filter: an
699 alternative to ensemble square root filters. *Tellus* 60A, 361–371.
- 700 Sakov P., Counillon F., Bertino L., Lisæter K. A., Oke P. R., & Korablev A. 2012. TOPAZ4: an
701 ocean-sea ice data assimilation system for the North Atlantic and Arctic. *Ocean Sci.* 8,
702 633-656, doi:10.5194/os-8-633-2012.
- 703 Sato K. & Inoue J. 2017. Comparison of Arctic sea ice thickness and snow depth estimates from
704 CFSR with in situ observations. *Clim. Dyn.* 1-13, doi:10.1007/s00382-017-3607-z.
- 705 Schøyen H., & Bråthen S. 2011. The Northern Sea route versus the Suez Canal: cases from bulk
706 shipping. *J. Transp. Geogr.* 19, 977–983.
- 707 Screen J. A. 2017. Simulated Atmospheric Response to Regional and Pan-Arctic Sea Ice Loss. *J.*

708 Climate 30, 3945–3962, <https://doi.org/10.1175/JCLI-D-16-0197.1>

709 Schweiger A., Lindsay R., Zhang J., Steele M., Stern H., & Kwok R. 2011. Uncertainty in modeled
710 Arctic sea ice volume. *J. Geophys. Res.* 116, C00D06, doi:10.1029/2011JC007084.

711 Schweiger A. J., & Zhang J. 2015. Accuracy of short-term sea ice drift forecasts using a coupled
712 ice-ocean model. *J. Geophys. Res. Oceans* 120, 7827–7841, doi:10.1002/2015JC011273.

713 Semtner A. 1976. A Model for the Thermodynamic Growth of Sea Ice in Numerical Investigations
714 of Climate. *J. Phys. Oceanogr.* 6, 379–389.

715 Serreze M. C. & Barry R. G. 1988. Synoptic activity in the Arctic basin, 1979–85. *J. Climate* 1,
716 1276–1295.

717 Serreze M. C. & Barrett A. P. 2008. The summer cyclone maximum over the central Arctic Ocean.
718 *J. Climate* 21, 1048–1065.

719 Simonsen M., Hackett B., Bertino L., Røed L. P., Waagbø G. A., Drivdal M., Sutherland G. 2017.
720 PRODUCT USER MANUAL For Arctic Ocean Physical and Bio Analysis and Forecasting
721 Products 5.5. EU, Copernicus Marine Service, <http://marine.copernicus.eu> pp. 56.

722 Simmonds I. & Rudeva I. 2012. The great Arctic cyclone of August 2012. *Geophys. Res. Lett.* 39,
723 L23709, <https://doi.org/10.1029/2012GL054259>.

724 Stark J. D., Ridley J., Martin M., & Hines A. 2008. Sea ice concentration and motion assimilation
725 in a sea ice–ocean model. *J. Geophys. Res.* 113, C05S91, doi:10.1029/2007JC004224.

726 Steele M. Ermold W., & Zhang J. 2008. Arctic Ocean surface warming trends over the past 100
727 years. *Geophys. Res. Lett.* 35, L02614, doi:10.1029/2007GL031651.

728 Stroeve J., Hamilton L. C., Bitz C. M., & Blanchard-Wrigglesworth E. 2014. Predicting September
729 sea ice: Ensemble skill of the SEARCH Sea Ice Outlook 2008–2013. *Geophys. Res. Lett.* 41,
730 2411–2418, doi:10.1002/2014GL059388.

731 Tan X., Su K., Riska K., & Moan T. 2013. A six-degrees-of-freedom numerical model for level ice–
732 ship interaction. *Cold Reg. Sci. Technol.* 92, 1–16, doi:10.1016/j.coldregions.2013.03.006.

733 Thorndike A. S. & Colony R. 1982. Sea ice motion in response to geostrophic winds. *J. Geophys.*
734 *Res.* 87, 5845–5852, doi:10.1029/JC087iC08p05845.

735 Wang W., Chen M., & Kumar A. 2013. Seasonal Prediction of Arctic Sea Ice Extent from a
736 Coupled Dynamical Forecast System. *Mon. Wea. Rev.* 141, 1375–1394, doi:
737 10.1175/MWR-D-12-00057.1.

738 Wang X., Key J., Kwok R., & Zhang J. 2016. Comparison of Arctic Sea ice thickness from
739 satellites, aircraft, and PIOMAS data. *Remote Sens.* 8, 713, doi:10.3390/rs8090713.

740 Wassmann P. 2011. Arctic marine ecosystems in an era of rapid climate change. *Prog. Oceanogr.* 90,
741 1–17.

742 Xie J., Bertino L., Counillon F., Lisæter K. A., & Sakov P. 2017. Quality assessment of the
743 TOPAZ4 reanalysis in the Arctic over the period 1991–2013. *Ocean Sci.* 13, 123–144,
744 doi:10.5194/os-13-123-2017.

745 Yamagami A., Matsueda M., & Tanaka H. L. 2017. Extreme Arctic cyclone in August 2016.
746 *Atmosph. Sci. Lett.* 18: 307–314. doi: 10.1002/asl.757.

747 Yamagami A., Matsueda M., & Tanaka H. L. 2018. Predictability of the 2012 great Arctic cyclone
748 on medium-range timescales, [15, 13-23](#), doi: [10.1016/j.polar.2018.01.002](#) *Polar Sci.* (in press).

749 Yamamoto-Kawai M., McLaughlin F. A., & Carmack E. C. 2011. Effects of ocean acidification,
750 warming and melting of sea ice on aragonite saturation of the Canada Basin surface water.
751 *Geophys. Res. Lett.* 38, L03601, doi:10.1029/2010GL045501.

752 Yamazaki A., Inoue J., Dethloff K., Maturilli M., & König-Langlo G. 2015. Impact of radiosonde
753 observations on forecasting summertime Arctic cyclone formation. *J. Geophys. Res.* 120,
754 3249–3273, doi:10.1002/2014JD022925.

755 Zhang J. & Rothrock D. A. 2003. Modeling global sea ice with a thickness and enthalpy
756 distribution model in generalized curvilinear coordinates. *Mon. Wea. Rev.* 131, 681–697.

757

758 **Table 1.** List of observed and simulated sea ice thickness datasets

Data sources		Period	Spatial resolution	Time step
TOPAZ4	Reanalysis	2011–2014	12.5 km	Daily
	Forecast	2013–2016	12.5 km	Daily
CS2SMOS		2011–2014 (October to April)	~25 km	7 days
IMB	2011K	1 September 2011 to 14 May 2012	Point-wise	Hourly
	2012I	14 August 2012 to 21 December 2012		
	2012J	25 August 2012 to 3 August 2013		
	2014B	26 March to 29 July 2014		
PIOMAS		2011–2014	~0.8°	Daily

759

760 **Table 2.** Pattern correlations ~~of between~~ monthly mean climatologies of SIT in [TOPAZ4](#) with those
761 [in PIOMAS and CS2SMOS](#), ~~and the TOPAZ4 and PIOMAS models~~ over the Arctic marginal seas
762 (Laptev, East Siberian, and Chukchi Seas)

Month	Mar.	Apr.	May	Jun.	Jul.
PIOMAS	0.92 0.87	0.93 0.86	0.93 0.84	0.92 0.71	0.92 0.49
CS2SMOS	0.86 0.53	0.82 0.35	–	–	–

763

764 **Table 3.** Monthly mean ~~SIT~~ biases ~~of TOPAZ4 SIT in the ESS~~ relative to [the CS2SMOS and](#)
765 [PIOMAS SIT data](#) ~~observed SIT averaged over the ESS~~

SIT bias (cm)	Mar.	Apr.	May	Jun.	Jul.
CS2SMOS	-23	<1	-	-	-
PIOMAS	-65	-63	-56	-23	21

766

767 **Figure captions**

768 **Figure 1.** Spatial distribution of climatological monthly mean of SIT (cm) in July during 2011–
769 2014: (a) PIOMAS, (b) TOPAZ4 reanalysis, and (c) their difference (cm). The boundaries of the
770 ESS and Arctic marginal seas are indicated in panel a by thick and thin lines, respectively. In panel
771 a, the trajectories of IMB buoys for 2011K, 2012I, 2012J, and 2014B (see Table 1 for the details of
772 each buoy data) are shown by black, red, blue and green dots, respectively.

773 **Figure 2.** Spatial distribution of climatological monthly mean of SIT (cm) in April during 2011–
774 2014: (top) CS2SMOS, (middle) TOPAZ4 reanalysis, and (bottom) their difference (cm).

775 **Figure 3.** Time series of daily mean SIT (cm) averaged over the ESS (rectangular region denoted
776 by black line in Fig. 1 (a)) derived from CS2SMOS (black), TOPAZ4 reanalysis (red), and
777 PIOMAS (blue) from January 2011 to August 2014. For CS2SMOS data, 7 day mean values are
778 shown. The standard deviations of area-averaged data are shown by vertical lines, respectively. The
779 ice types (2: first-year ice, 3: multi-year ice) used for the choice of satellite SIT retrievals in
780 CS2SMOS are shown by green bar. The scale for the ice type is located on the right vertical axis.

781 **Figure 4.** The comparisons of the daily mean SITs derived from IMB buoy data with the
782 corresponding SIT in TOPAZ4 reanalysis data from 2011 to 2014 in and around the ESS. The SIT
783 data are re-sampled per 7 days. The regression lines onto IMB buoy data and the reference unit line
784 are shown by solid and dashed lines, respectively.

785 **Figure 5.** Spatial distribution of (a) monthly mean (colors) climatological SIT (m) in the TOPAZ4
786 reanalysis and (b) the RMS variability of daily mean SIT (colors) in July during 2011–2014. The
787 monthly mean of climatological SIC (white contours) in July is indicated in panel (a). The
788 rectangular region enclosing the ESS (70°–80°N, 150°–180°E) is shown in panel (b). (c) Time
789 series of monthly mean SIT (grey shade) and RMS of TOPAZ4 reanalysis (black line) averaged
790 over the ESS. The scale of the RMS is indicated on the right axis.

791 **Figure 6.** The prediction skill (PCC) of SIT forecast in the ESS (70°–80°N, 150°–180°E) in each

792 month obtained from (a) operational forecast model and (b) persistency of the initial value,
793 averaged from 2014–2016. The standard deviations of the PCCs are shown with white contours. In
794 panel c, the fraction of variance explained by operational forecast relative to the persistency (%) is
795 shown by contour (the region where the fraction is larger than 10% is shaded).

796 **Figure 7.** PCCs between forecast and analysis (a) SIT, (b) zonal and meridional ice speed, and (c)
797 zonal and meridional surface wind speed from operational TOPAZ4 data in early summer
798 (June–July) averaged on 2014–2016. Error bar indicates the standard deviation of the PCCs.

799 **Figure 8.** Temporal evolution of SIT (cm; colors) and ice velocity (m s^{-1} ; vectors) distribution for
800 (left) analysis, (center) forecast, and (right) the difference between forecast and analysis at
801 increasing lead times from +0 day to +6 days initialized on 2nd July 2015. The corresponding PCCs
802 for the SIT (black), zonal (red) and meridional ice speeds (blue) in the ESS (right-lower panel of the
803 time evolution) are shown in the lower panel. The scale for the PCCs of the zonal and meridional
804 ice speeds is indicated on the right axis.

805 **Figure 9.** (a) Relationship between 10m wind speed (m s^{-1}) in the ERA Interim reanalysis data and
806 sea ice speed (m s^{-1}) in the TOPAZ4 reanalysis averaged over a part of the ESS (72° – 76° N,
807 150° – 170° E) during 1–31 July 2011–2014. Broken and solid lines indicate the regression line of
808 ice speed on 10m wind speed ($y = 0.0224x - 0.0112$) and the theoretical ice speed estimated based
809 on classical free-drift theory, respectively. (b) Angle (degrees) of sea ice velocity relative to surface
810 wind vectors averaged over the ESS. Positive values indicate sea ice drift is to the right of the wind
811 direction. Solid curve indicates the wind–ice velocity angle estimated based on classical free-drift
812 theory.

813 **Figure 10.** The PCCs between forecast and analysis SIT from the full physics model (black),
814 persistency (red), and a simple melting model (blue) in early summer (June–July) averaged from
815 2014–2016. Error bar indicates the standard deviation of the PCCs.

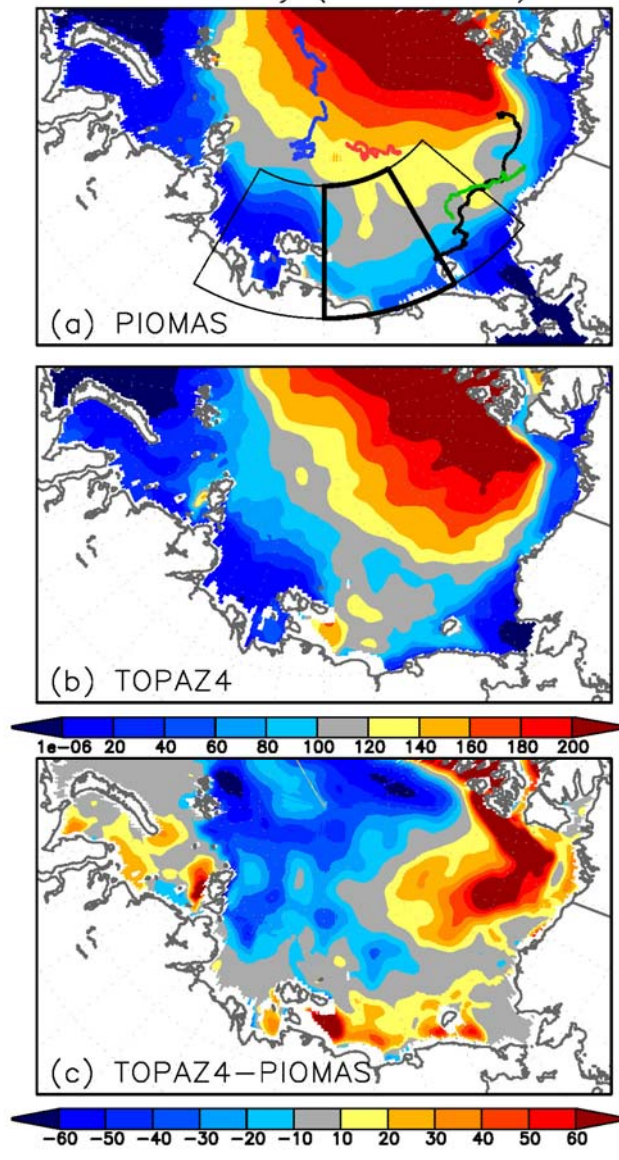
816 **Figure 11.** Temporal evolution of SIT differences (cm; colors) between the forecast and analysis
817 data at lead times increasing from +2 to +8 days, initialized on 2nd July 2015. In each panel, the sea
818 ice edge of the analysis, defined by 30% SIC, is shown. Corresponding PCCs for the full physics
819 model (black), a simple melting model (red) and persistency (blue) in the ESS (right-lower panel of
820 the time evolution) are shown in the lower panel.

821 **Figure 12.** Trajectory of the two tankers over the ESS based on AIS data. The routes cross the ESS
822 from the Laptev Sea on 4 July 2014 to the port of Yamal on 31 July 2014, via the port of Pevek on
823 20 July 2014. The forward route is highlighted by green circles. The SIT (cm; colors) and SIC (%;
824 contours) averaged over the period of the forward route are shown.

825 **Figure 13.** Scatter plots of hourly vessel speeds (knots) and (a) daily mean SIT (cm) and (b) SIC
826 (%) in TOPAZ4 reanalysis from 4–30 July 2014. In each panel, the regression line of vessel speed
827 onto each variable is shown by broken line.

828

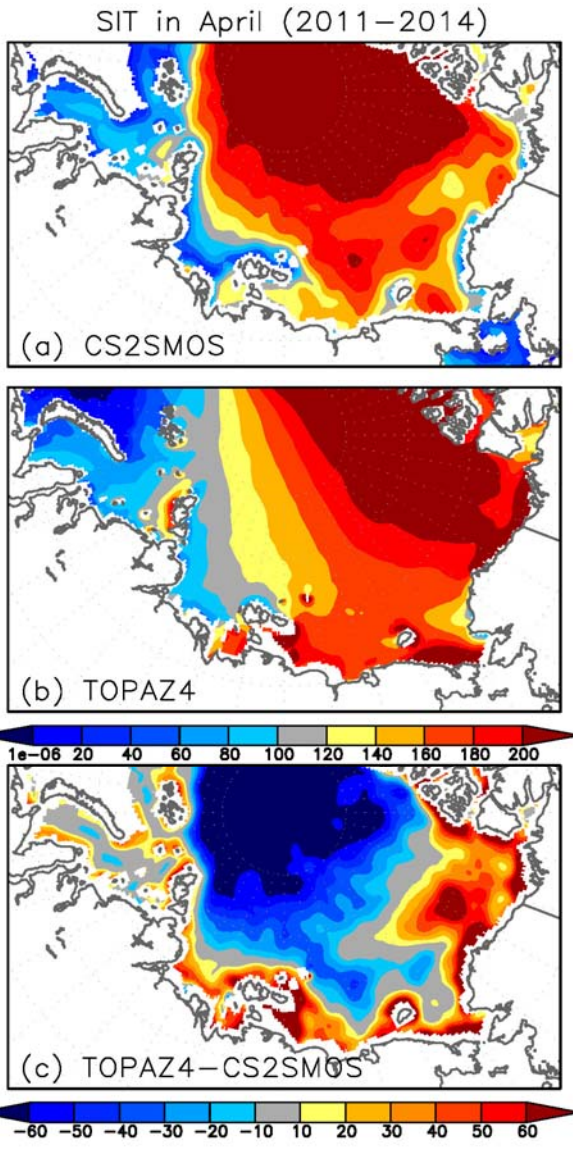
SIT in July (2011–2014)



829

830 **Figure 1.** Spatial distribution of climatological monthly mean of SIT (cm) in April–July during
831 2011–2014: (aa) PIOMASCS2SMOS, (bb) TOPAZ4 reanalysis, and (ce) their difference (cm). The
832 boundariesboundaries of the ESS and Arctic marginal seas are ~~and Arctic marginal seas are~~
833 indicated in panel apanel ~~by thick and thin lines, respectively~~ by thick and thin lines,
834 respectively. In panel a, the trajectories of IMB buoys for 2011K, 2012I, 2012J, and 2014B (see
835 Table 1 for the details of each buoy data) are shown by black, red, blue and green dots, respectively.

836

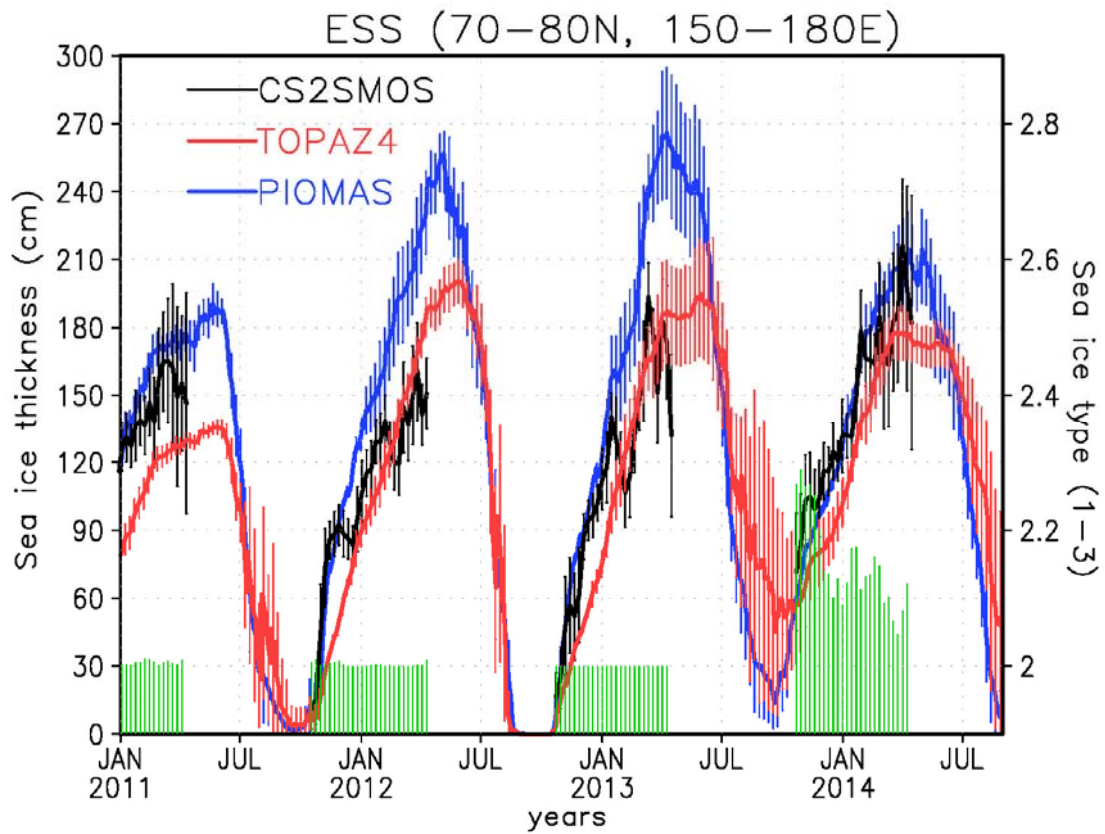


837

838

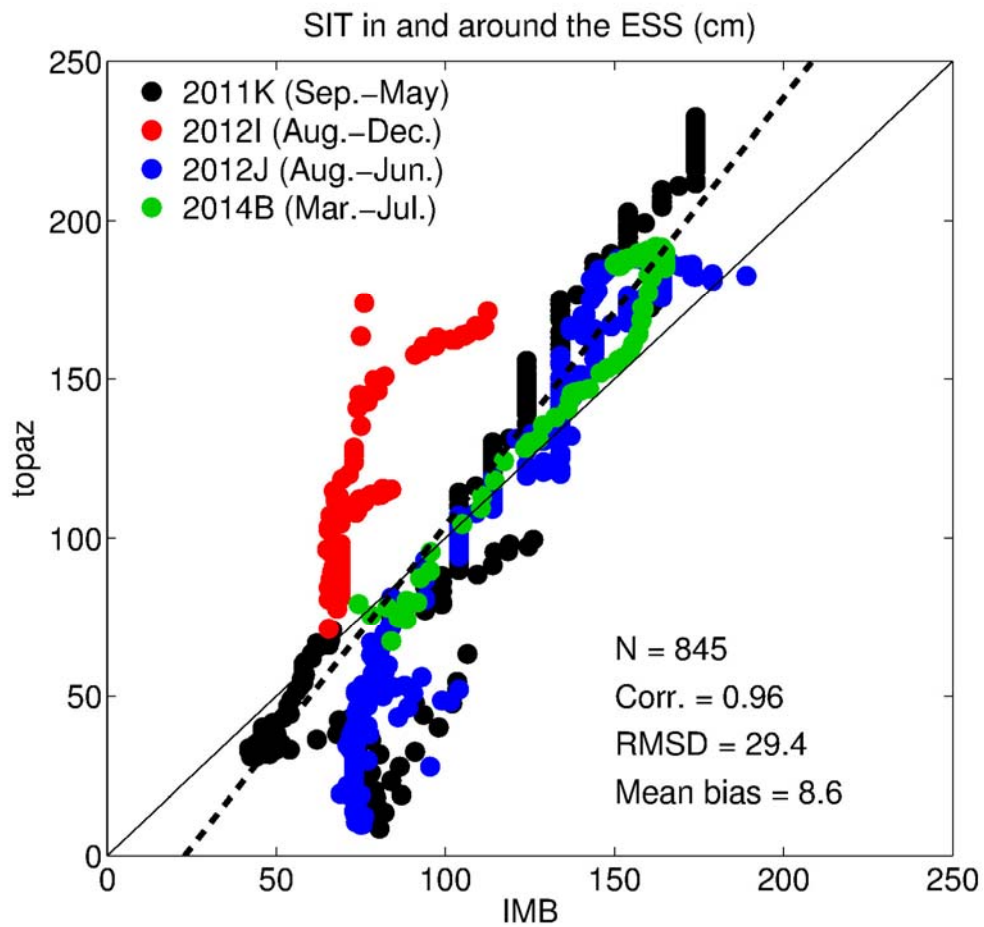
839

Figure 2. Spatial distribution of climatological monthly mean of SIT (cm) in April during 2011–2014: (top) CS2SMOS, (middle) TOPAZ4 reanalysis, and (bottom) their difference (cm).



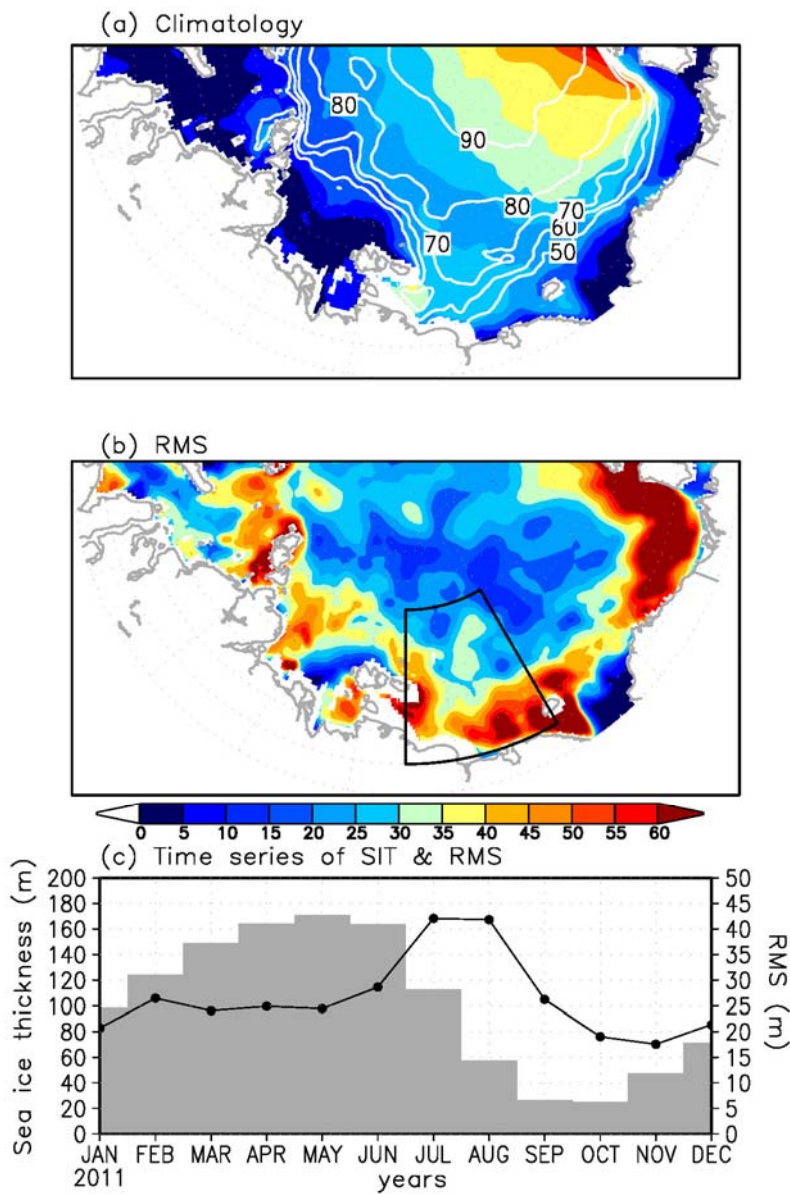
840

841 **Figure 32.** Time series of daily mean SIT (cm) averaged over the ESS (rectangular region denoted
 842 by black line in Fig. 1 (a)) derived from CS2SMOS (black), TOPAZ4 reanalysis (red), and
 843 PIOMAS (blue) from January 2011 to August 2014. For CS2SMOS data, 7 day mean values are
 844 shown. The standard deviations of area-averaged data are shown by vertical lines, respectively. The
 845 ice types (2: first-year ice, 3: multi-year ice) used for the choice of satellite SIT retrievals in
 846 CS2SMOS are shown by green bar. The scale for the ice type is located on the right vertical axis.



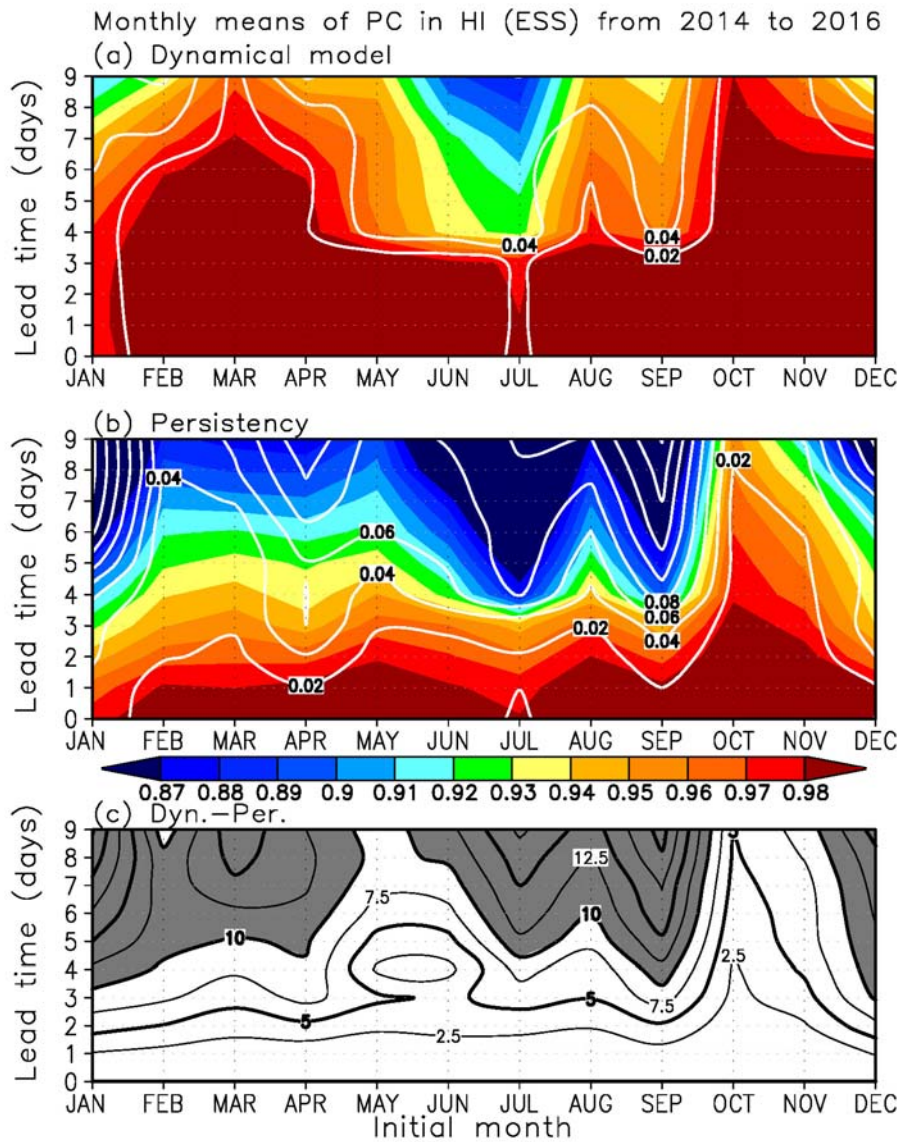
847

848 [Figure 4.](#) The comparisons of the daily mean SITs derived from IMB buoy data with the
849 [corresponding SIT in TOPAZ4 reanalysis data from 2011 to 2014 in and around the ESS.](#) The SIT
850 [data are re-sampled per 7 days.](#) The reference unit line and the regression lines onto IMB buoy data
851 [are shown by solid and dashed lines, respectively.](#)



852

853 **Figure 54.** Spatial distribution of (a) monthly mean (colors) climatological SIT (m) in the TOPAZ4
 854 reanalysis and (b) the RMS variability of daily mean SIT (colors) in July during 2011–2014. The
 855 monthly mean of climatological SIC (white contours) in July is indicated in panel (a). The
 856 rectangular region enclosing the ESS (70°–80°N, 150°–180°E) is shown in panel (b). (c) Time
 857 series of monthly mean SIT (grey shade) and RMS of TOPAZ4 reanalysis (black line) averaged
 858 over the ESS. The scale of the RMS is indicated on the right axis.



859

860

861

862

863

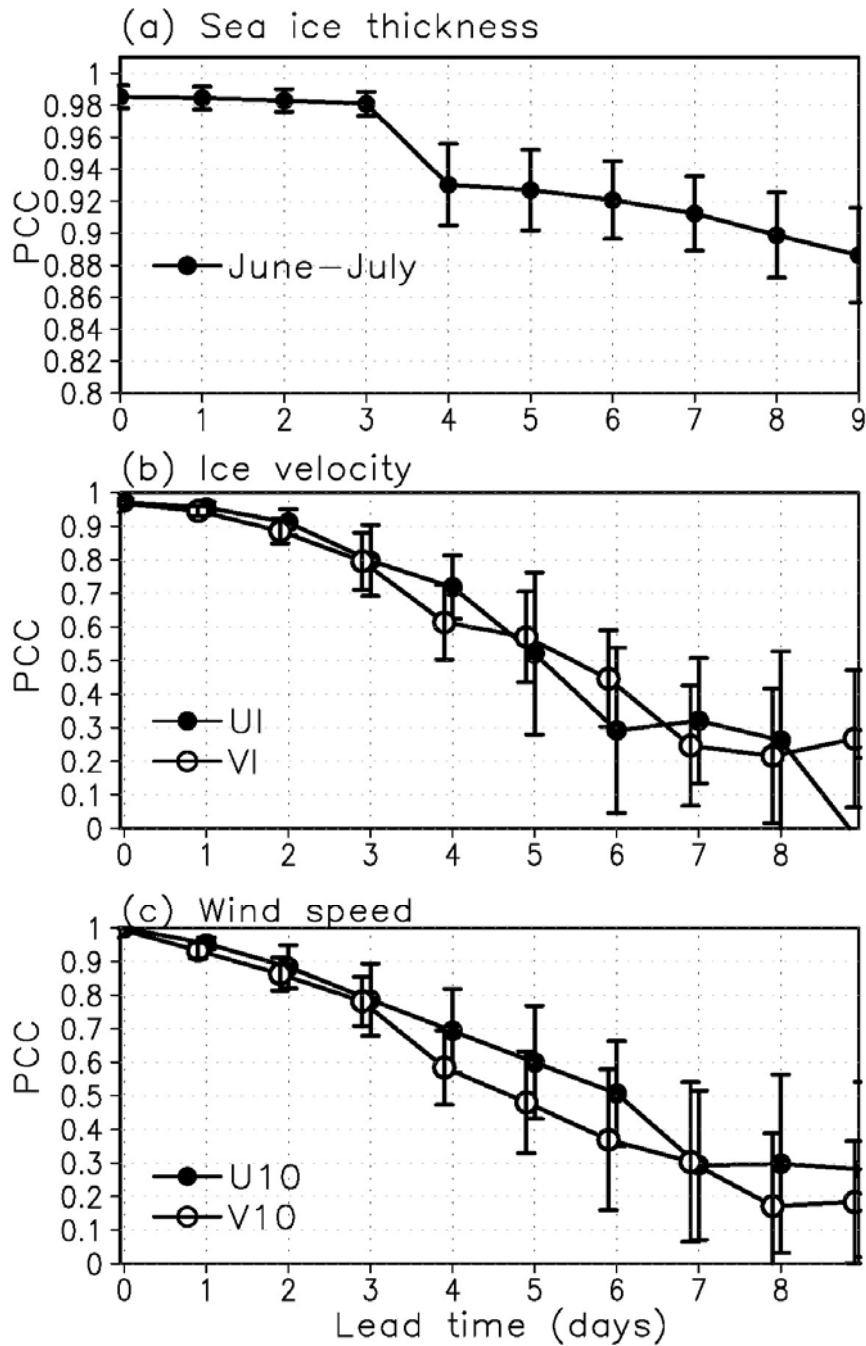
864

865

866

867

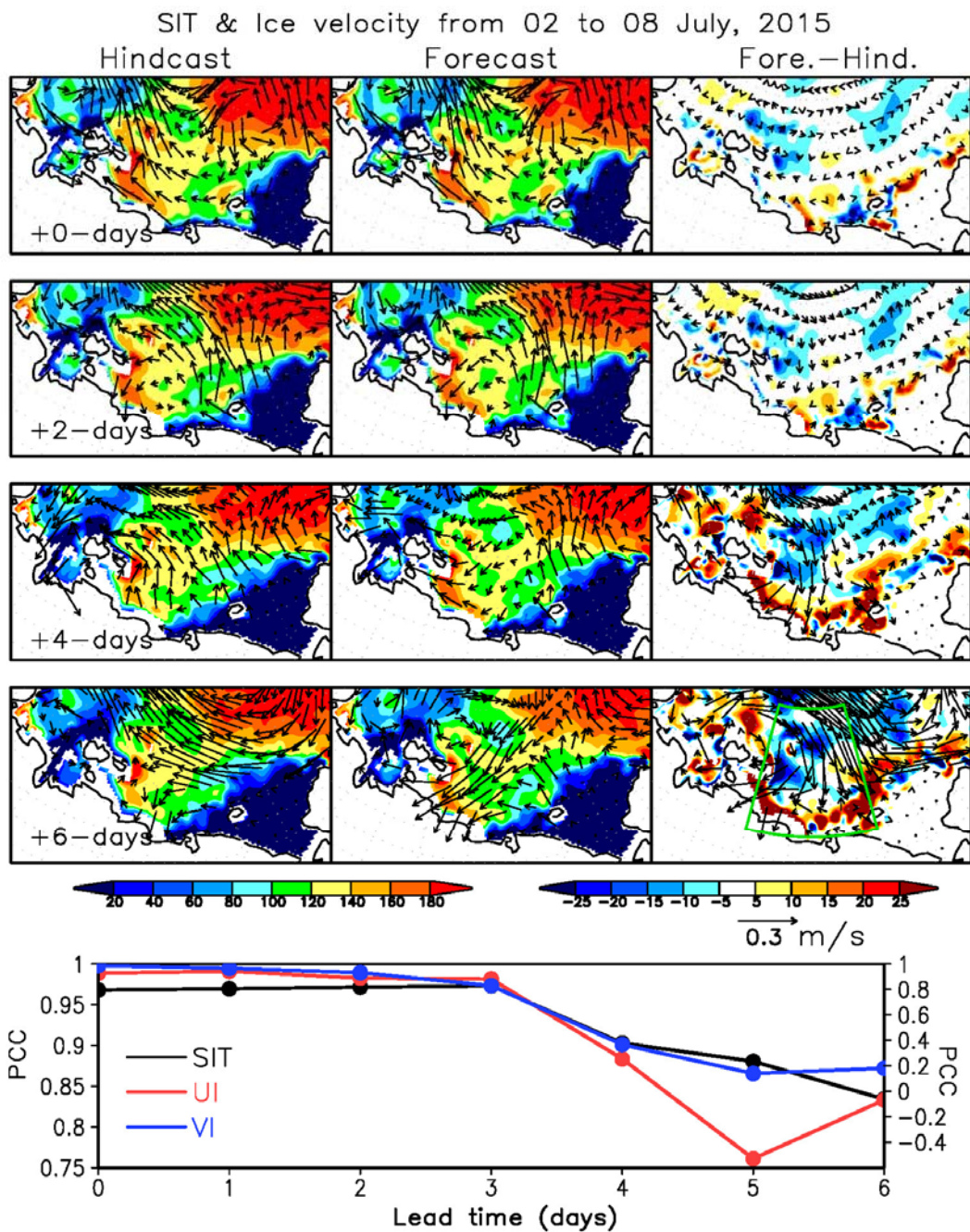
Figure 65. The prediction skill (PCC) of SIT forecast in the ESS (70°–80°N, 150°–180°E) in each month obtained from (a) operational forecast model and (b) persistency of the initial value, averaged from 2014–2016. The standard deviations of the PCCs are shown with white contours. In panel c, the fraction of variance explained by operational forecast relative to the persistency (%) is shown by contour (the region where the fraction is larger than 10% is shaded). The PCCs (colors) between operational forecast and analysis SIT in the ESS (70°–80°N, 150°–180°E) in each month, averaged from 2013–2016. The isoline of standard deviation of the PCCs at 0.05 is shown with white contours.



869

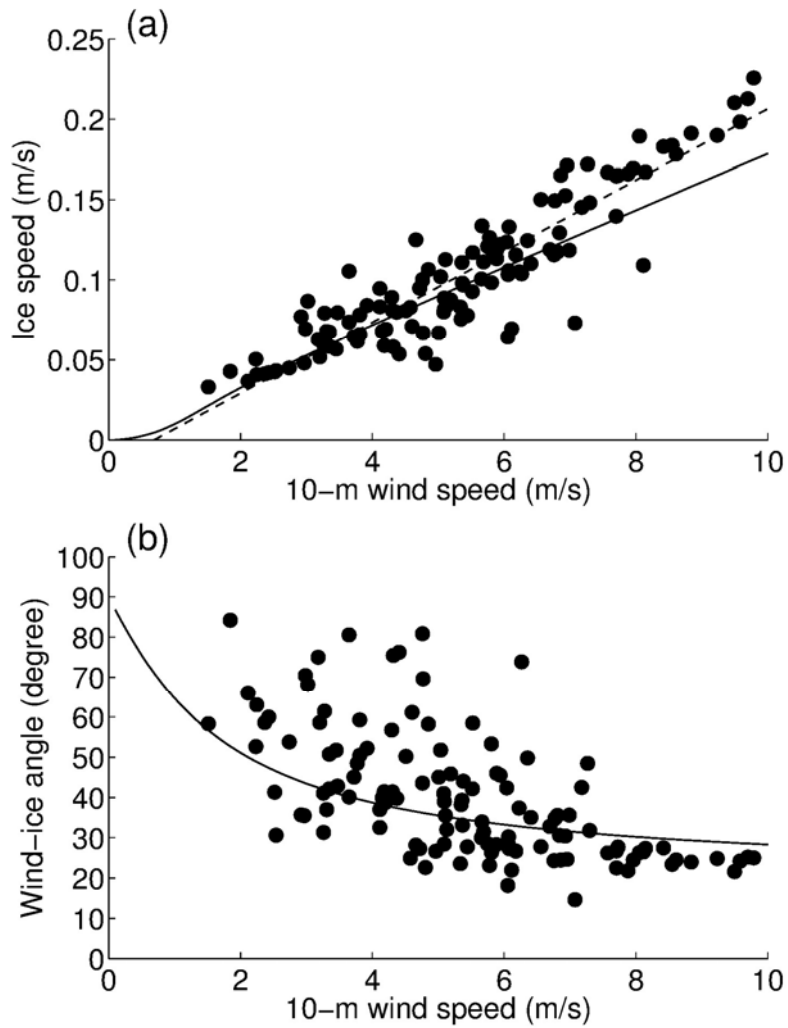
870 **Figure 76.** PCCs between forecast and analysis [\(a\) SIT](#), [\(b\) zonal and meridional ice speed](#), and [\(c\)](#)
 871 [zonal and meridional surface wind speed](#) from operational TOPAZ4 data in early summer
 872 (June–July) averaged on ~~2014–2016~~[2013–2016](#). Error bar indicates the standard deviation of the
 873 PCCs.

874



875

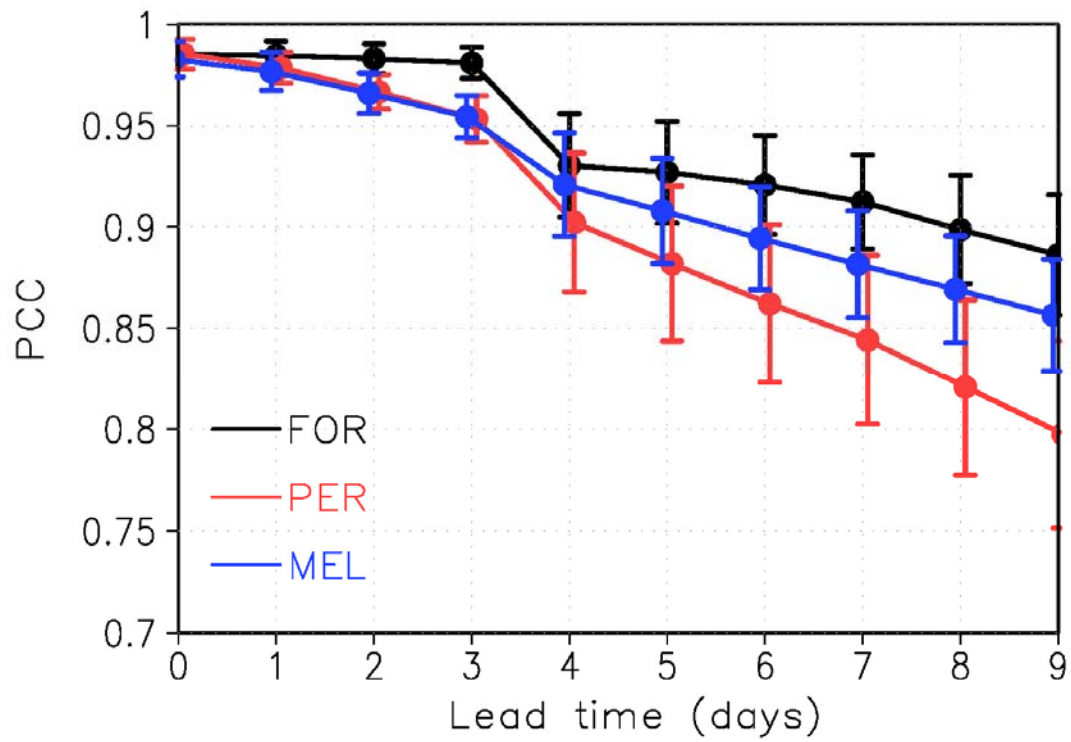
876 **Figure 8.** Temporal evolution of SIT (cm; colors) and ice velocity (m s^{-1} ; vectors) distribution for
 877 (left) analysis, (center) forecast, and (right) the difference between forecast and analysis at
 878 increasing lead times from +0 day to +6 days initialized on 2nd July 2015. The corresponding PCCs
 879 for the SIT (black), zonal (red) and meridional ice speeds (blue) in the ESS (right-lower panel of the
 880 time evolution) are shown in the lower panel. The scale for the PCCs of the zonal and meridional
 881 ice speeds is indicated on the right axis.



882

883 **Figure 9.** (a) Relationship between 10m wind speed (m s^{-1}) in the ERA Interim reanalysis data and
 884 sea ice speed (m s^{-1}) in the TOPAZ4 reanalysis averaged over a part of the ESS (72° – 76° N,
 885 150° – 170° E) during 1–31 July 2011–2014. Broken and solid lines indicate the regression line of
 886 ice speed on 10m wind speed ($y = 0.0224x - 0.0112$) and the theoretical ice speed estimated based
 887 on classical free-drift theory, respectively. (b) Angle (degrees) of sea ice velocity relative to surface
 888 wind vectors averaged over the ESS. Positive values indicate sea ice drift is to the right of the wind
 889 direction. Solid curve indicates the wind–ice velocity angle estimated based on classical free-drift
 890 theory.

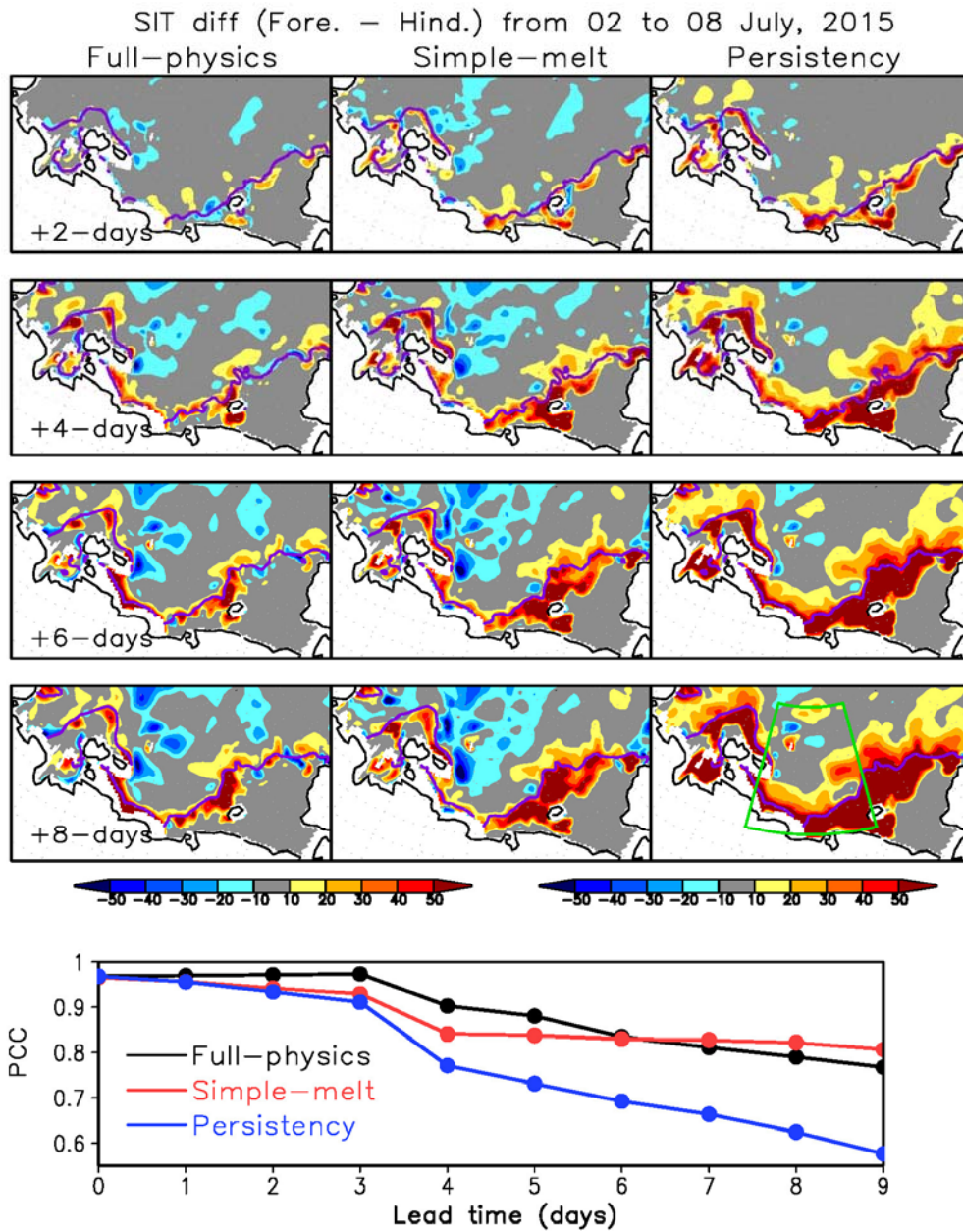
891



892

893 **Figure 10.** The PCCs between forecast and analysis SIT from the full physics model (black),
 894 persistency (red), and a simple melting model (blue) in early summer (June–July) averaged from
 895 2014~~2013~~–2016. Error bar indicates the standard deviation of the PCCs.

896

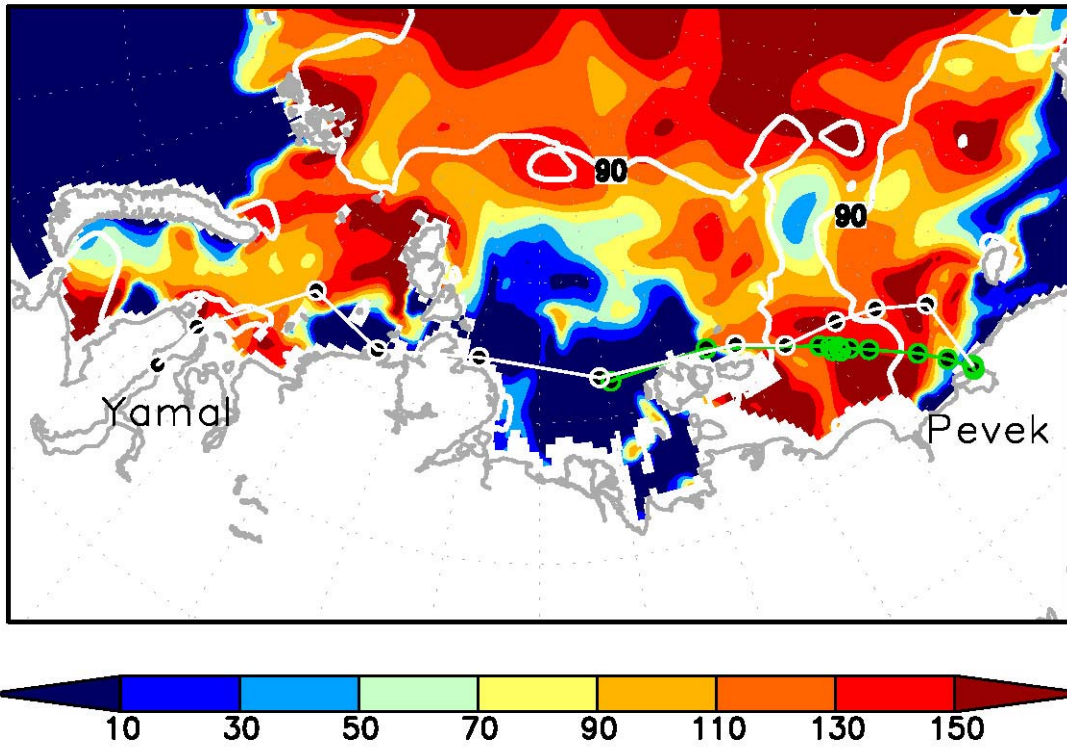


897

898 **Figure 11.** Temporal evolution of SIT differences (cm; colors) between the forecast and analysis
 899 data at lead times increasing from +2 to +8 days, initialized on 2nd July 2015. In each panel, the sea
 900 ice edge of the analysis, defined by 30% SIC, is shown. Corresponding PCCs for the full physics
 901 model (black), a simple melting model (red) and persistency (blue) in the ESS (right-lower panel of
 902 the time evolution) are shown in the lower panel.

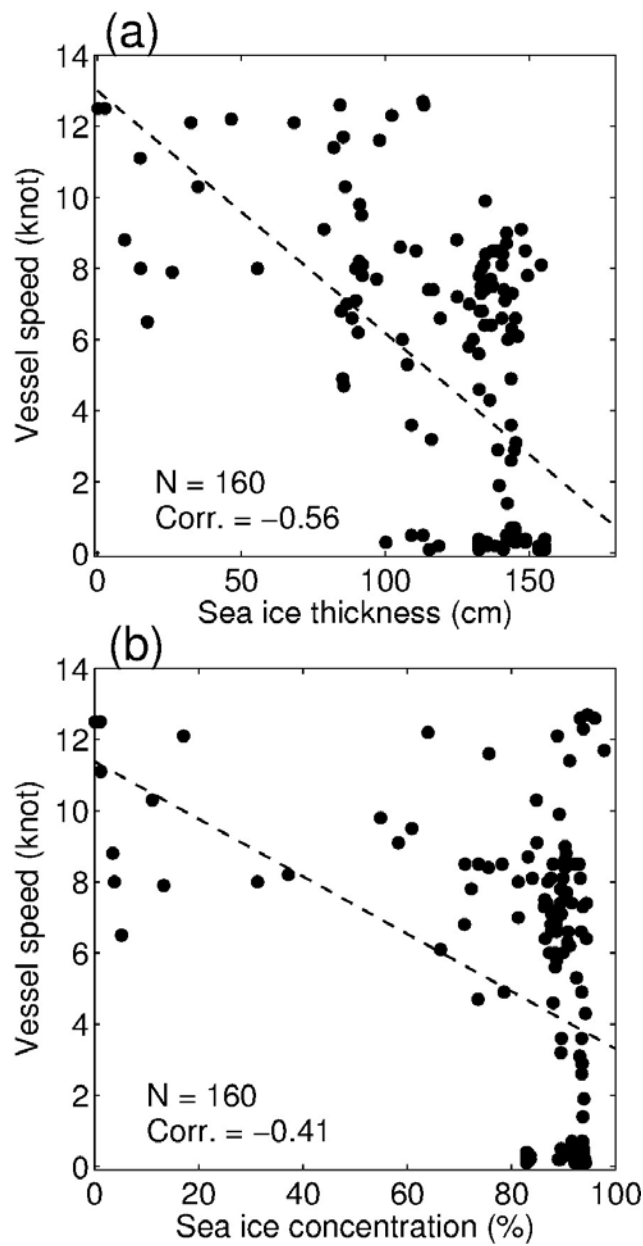
903

TOPAZ4-SIT & SIC in 04-15JUL2014



904

905 **Figure 12.** Trajectory of the two tankers over the ESS based on AIS data. The routes cross the ESS
906 from the Laptev Sea on 4 July 2014 to the port of Yamal on 31 July 2014, via the port of Pevek on
907 20 July 2014. The forward route is highlighted by green circles. The SIT (cm; colors) and SIC (%;
908 contours) averaged over the period of the forward route are shown.



909

910 **Figure 13.** Scatter plots of hourly vessel speeds (knots) and (a) daily mean SIT (cm) and (b) SIC

911 (%) in TOPAZ4 reanalysis from 4–30 July 2014. In each panel, the regression line of vessel speed

912 onto each variable is shown by broken line. ~~Scatter plots of daily mean vessel speeds (knots) and sea~~

913 ~~ice thickness (cm) from 4–30 July 2014.~~